DMD Fast Forward. Published on November 20, 2012 as doi: 10.1124/dmd.112.049684
This article has not been copyedited and formatted. The final version may differ from this version.

DMD #49684

Metabolism and Pharmacokinetics of 3-*n*-Butylphthalide (NBP) in Humans: The Role of Cytochrome P450s and Alcohol Dehydrogenase in Biotransformation

Xingxing Diao, Pan Deng, Cen Xie, Xiuli Li, Dafang Zhong, Yifan Zhang and Xiaoyan Chen

Shanghai Institute of Materia Medica, Chinese Academy of Sciences, Shanghai, China

(X. D., P. D., C. X., X. L., D. Z., Y. Z., X. C.)

DMD Fast Forward. Published on November 20, 2012 as DOI: 10.1124/dmd.112.049684
This article has not been copyedited and formatted. The final version may differ from this version.

Running Title

Metabolism and Pharmacokinetics of NBP in Humans

Corresponding Author: Xiaoyan Chen

Shanghai Institute of Materia Medica, Chinese Academy of Sciences, 501 Haike Road, Shanghai, 201203, China;

Phone: +86-21-50800738; Fax: 0086-21-50800738;

Email: xychen@mail.shcnc.ac.cn

Number of text pages: 33

Number of tables: 4

Number of figures: 8

Number of references: 39

Number of words in the Abstract: 246

Number of words in the Introduction: 395

Number of words in the Discussion: 1026

ABBREVIATIONS: ABT, 1-aminobenzotriazole; ADH, alcohol dehydrogenase; ALDH, aldehyde dehydrogenase; AUC, area under the concentration–time curve; CYP450s, cytochrome P450s; ESI, electrospray; FMOs, Flavin-containing monooxygenases; HLMs, human liver microsomes; MDF, mass defect filter; 4-MP, 4-methylpyrazole; NADPH, reduced form of nicotinamide adenine dinucleotide phosphate; NAD, nicotinamide adenine dinucleotide; NBP, 3-*n*-butylphthalide; NMR, nuclear magnetic resonance; 17-ODYA, 17-octadecynoic acid; 4-PA, 4-pentenoic acid; Q-TOF MS, quadrupole time-of-flight mass spectrometry; SKF525A, proadifen; UDPGA, uridine 5'-diphosphoglucuronic acid; UPLC, ultra-performance liquid chromatography; UV, ultraviolet.

DMD Fast Forward. Published on November 20, 2012 as DOI: 10.1124/dmd.112.049684
This article has not been copyedited and formatted. The final version may differ from this version.

ABSTRACT:

3-*n*-Butylphthalide (NBP) is a cardiovascular drug currently used for the treatment of cerebral ischemia. The present study aims to investigate the metabolism, pharmacokinetics, and excretion of NBP in humans and identify the enzymes responsible for the formation of major metabolites. NBP underwent extensive metabolism after an oral administration of 200 mg NBP and 23 metabolites were identified in human plasma and urine. Principal metabolic pathways included hydroxylation on alkyl side chain, particularly at 3-, ω-1-, and ω- carbons, and further oxidation and conjugation. Approximately 81.6% of the dose was recovered in urine, mainly as NBP-11-oic acid (M5-2) and glucuronide conjugates of M5-2 and mono-hydroxylated products. 10-Keto-NBP (M2), 3-hydroxy-NBP (M3-1), 10-hydroxy-NBP (M3-2), and M5-2 were the major circulating metabolites, wherein the areas under the curve values were 1.6-, 2.9-, 10.3-, and 4.1-fold higher than that of NBP. Reference standards of these four metabolites were obtained through microbial biotransformation by *Cunninghamella blakesleana*. In vitro phenotyping studies demonstrated that multiple cytochrome P450s (CYP450s) isoforms, especially CYP3A4, 2E1, and 1A2, were involved in the formation of M3-1, M3-2, and 11-hydroxy-NBP. Using M3-2 and 11-hydroxy-NBP as substrates, human subcellular fractions experiments revealed that CYP450s, alcohol dehydrogenase, and aldehyde dehydrogenase catalyzed the generation of M2 and M5-2. Formation of M5-2 was much faster than that of M2, and M5-2 can undergo β-oxidation to yield phthalide-3-acetic acid in rat liver homogenate. Overall, our study demonstrated that

DMD Fast Forward. Published on November 20, 2012 as DOI: 10.1124/dmd.112.049684
This article has not been copyedited and formatted. The final version may differ from this version.

NBP was well absorbed and extensively metabolized by multiple enzymes to various metabolites prior to urinary excretion.

DMD Fast Forward. Published on November 20, 2012 as DOI: 10.1124/dmd.112.049684
This article has not been copyedited and formatted. The final version may differ from this version.

Introduction

3-*n*-Butylphthalide (NBP), [(±)-3-butyl-1(3H)-isobenzofuranone], is a potent and widely used drug for the treatment of ischemic stroke in clinic. Racemic NBP has been approved for marketing in 2004 by the State Food and Drug Administration (SFDA) of China in the form of soft capsule and infusion drip. The recommended dose of NBP is 200 mg, taken three times a day. Previous pharmacological studies have demonstrated that NBP exhibits neuroprotective effects by increasing the regional cerebral blood flow in the ischemic zone and inhibiting the release of glutamate and 5-hydroxytryptamine (Yan and Feng, 1998; Yan et al., 1998; Chong and Feng, 1999; Xu and Feng, 2001). Recent studies have revealed that NBP displays beneficial effects in attenuating amyloid-induced cell death in neuronal cultures, improving cognitive impairment in an animal model of Alzheimer's disease and preventing neuronal cell death after focal cerebral ischemia in mice via the c-Jun N-terminal kinase pathway (Peng et al., 2008; Li et al., 2010; Peng et al., 2010).

Although the pharmacological properties of NBP were intensively investigated, its absorption, distribution, metabolism, and excretion are not well understood; only a few studies have investigated its metabolism in rats (Peng and Zhou, 1996; Wang et al., 1997). Based on the fragmentation of tentative metabolites and their tetramethylsilane derivatives, four hydroxylated metabolites were observed in the urine after an oral administration in rat. In another in vivo study of radiolabeled ^{3}H-NBP, NBP was absorbed rapidly and metabolized extensively. The metabolites were mainly excreted in urine. One of the urinary metabolites was confirmed as

10-hydroxy-NBP, whereas the other metabolite was proposed to be 3-hydroxy-NBP without robust structure elucidation. To date, few studies have investigated the biotransformation of NBP in humans. Thus, a clear understanding of the metabolism of NBP in humans and the identification of the enzymes involved in its biotransformation would provide solid evidence for the safety evaluation of NBP, avoidance of potential drug-drug interaction, and inspiration for further discovery of new anti-stroke drugs (Li et al., 2011).

In light of these concerns, the present study aims to 1) investigate the metabolism of NBP in humans after an oral administration of 200 mg NBP soft capsules via ultra-performance liquid chromatography-ultraviolet/quadrupole time-of-flight mass spectrometry (UPLC-UV/Q-TOF MS); 2) characterize the pharmacokinetic and elimination profiles of NBP in humans; and 3) evaluate the roles of cytochrome P450s (CYP450s), alcohol dehydrogenase (ADH), aldehyde dehydrogenase (ALDH), and β-oxidation in NBP biotransformation.

DMD Fast Forward. Published on November 20, 2012 as DOI: 10.1124/dmd.112.049684
This article has not been copyedited and formatted. The final version may differ from this version.

Materials and methods

Materials. NBP was kindly provided by the China Shijiazhuang Pharmaceutical Group Co., Ltd (Shijiazhuang, Hebei, China). Phthalide-3-acetic acid was purchased from Alfa Aesar (Heysham, UK). Proadifen (SKF525A), 1-aminobenzotriazole (ABT), 4-methylpyrazole (4-MP), 17-octadecynoic acid (17-ODYA), and 4-pentenoic acid (4-PA) were purchased from Sigma-Aldrich Co. (St. Louis, MO). 11-Hydroxy-NBP, d_4-NBP, d_4-3-hydroxy-NBP, d_4-10-hydroxy-NBP, d_4-10-keto-NBP, and d_4-11-oic acid were synthesized in our laboratory using previously described methods with minor modifications (Brenstrum et al., 1994; Brimble et al., 1996; Yang et al., 2007). Pooled human liver microsomes (HLMs) and human liver cytosol from both genders, recombinant human P450 isoenzymes CYP1A2, 1B1, 2D6, and 4A11 without cytochrome b5 reductase, and CYP2A6, 2B6, 2C8, 2C9, 2C19, 2E1, 3A4, 3A5 with cytochrome b5 reductase were supplied by BD Gentest (Woburn, MA). The microbial strain *Cunninghamella blakesleana* ATCC9244 was obtained from the Institute of Microbiology, Chinese Academy of Sciences (Beijing, China). All solvents for LC-MS analysis were of high-performance liquid chromatography (HPLC) grade (Merck, Darmstadt, Germany). Other reagents were of analytical grade (Shanghai Chemical Plant, Shanghai, China). Ultra-pure water was generated using a Milli-Q Gradient system (Millipore Corporation, Molsheim, France).

Study Protocol and Sample Collection. This study is an open-labeled, nonrandomized single dose study. Four healthy Chinese male volunteers, aged 22 years to 26 years, with a mean body mass index of 21.65 kg/m^2 (ranging from 20.76

to 22.72), were enrolled in this study. The study protocol was approved by the Ethics Committee of the First Affiliated Hospital of Lanzhou University (Lanzhou, Gansu, China) and conducted in accordance with the Declaration of Helsinki and the principles of Good Clinical Practice. Written informed consents were obtained from all subjects prior to the study.

After an overnight fasting, the four healthy volunteers received an oral administration of 200 mg NBP soft capsules (China Shijiazhuang Pharmaceutical Group Co., Ltd, 100 mg/capsule, product lot: 11060211). Blood samples were collected pre-dose and at 0.25, 0.5, 1, 1.5, 2, 3, 4, 5, 8, 12, 24, 36, 48, and 72 h post-dose. The plasma samples were separated and stored at –20 °C until analysis. Urine and feces samples were collected pre-dose and at 0–12, 12–24, 24–48, 48–72 and 72–96 h post-dose. The total volume of the urine and total weight of the feces were recorded after each sample collection. The urine and feces samples were stored frozen at –20 °C until analysis.

Metabolite Profiling and Identification. *Preparation of Plasma and Urine Samples*. Human plasma and urine samples were pooled for metabolite profiling. Plasma samples were segregated by the sample collection time (0 h, 1 h, and 8 h), and equal volumes (150 μl) from each subject were pooled. Urine samples (0, 0–24, 24–48, 48–72, and 72–96 h) were pooled by combining the volumes proportional to the total volume excreted from each subject for each urine collection interval. For every 150 μl aliquot of pooled plasma (or urine) samples, 450 μl of acetonitrile were added. The mixture was mixed for 1 min and centrifuged for 5 min at 11,000 g. The supernatant

DMD Fast Forward. Published on November 20, 2012 as DOI: 10.1124/dmd.112.049684
This article has not been copyedited and formatted. The final version may differ from this version.

was then evaporated to dryness under nitrogen stream at 40 °C, and reconstituted in 75 μl (150 μl for urine samples) of methanol and water (10: 90, v/v). A 10 μl aliquot of the resulting solution (2 μl for urine samples) was injected for analysis.

Preparation of Feces Samples. Each feces sample was thawed and placed in 5 parts (1 g: 5 ml) methanol. The mixture was blended by a motor-driven homogenizer, and then the sample was vibrated by ultrasound wave for 15 min. A 20 ml aliquot of the mixture was removed and centrifuged at 3,500 g for 10 min. The 300-μl supernatant was transferred into another tube, evaporated to dryness under nitrogen stream at 40 ºC, and then reconstituted in 100 μl of methanol and water (10: 90, v/v). A 10 μl aliquot of the solution was injected for metabolite identification.

UPLC-UV/Q-TOF MS Analysis. Chromatographic separation for the metabolite profiling and identification was conducted on an Acquity UPLC HSS T3 column (100 mm × 2.1 mm i.d., 1.8 μm; Waters) using an Acquity UPLC system (Waters, Milford, MA). The mobile phase was a mixture of 5 mM ammonium acetate (A) and methanol (B). The gradient elution was maintained at 5% B for 3 min, increased linearly to 55% B over 15 min, to 100% B over the next 2 min and maintained for 1 min, and finally to 5% B for 3 min to reequilibrate the column. The flow rate was set at 0.4 ml/min, and the column temperature was set at 45 °C. The eluted fractions were monitored by UV detection at 230 nm.

MS detection was achieved using a Synapt Q-TOF high-resolution mass spectrometer (Waters, Milford, MA) operated in both positive and negative ion electrospray (ESI) modes. The desolvation gas was set to 700 l/h at 350 °C, with the

source temperature set at 100 °C. Data were centroided from 80 Da to 1000 Da during acquisition using an internal reference (400 ng/ml of leucine enkephalin) solution infused at 20 μl/min to generate a reference ion in ESI (+) mode at *m/z* 556.2771 and in ESI (–) mode at *m/z* 554.2615. MS^E function was programmed with independent low and high collision energies so that a low collision energy scan can be immediately followed by a high collision energy scan to induce the fragmentation of the ions transmitted through the quadrupole. Both intact precursor and fragment ions can be collected in a single run.

The UPLC and MS control were performed using the MassLynx 4.1 software (Waters). The blank and actual samples were processed using MetaboLynx, a subroutine of the MassLynx software integrated with the mass defect filtering (MDF) technology and Dealkylation tool to remove interferences from the matrix and facilitate the characterization of metabolites (Zhu, 2006; Zhang et al., 2009; Xie et al., 2012).

Isolation of Metabolites from Microbial Transformation. Frozen microbial stock culture of *C. blakesleana* ATCC9244 was first incubated in 250 ml flasks containing potato dextrose agar at 28 °C for 7 days in a rotary shaker set to 220 rpm (Asha and Vidyavathi, 2009; Deng et al., 2011). The seed culture (5.0 ml) was then inoculated into 250 ml flasks containing 50 ml of biotransformation medium consisting of dextrose (1.0 g), yeast extract (0.25 g), peptone (0.25 g), NaCl (0.25 g), and K_2HPO_4 (0.25 g). After incubation at 28 °C and 220 rpm for 24 h, NBP in methanol (10 mg/ml) was added for a final concentration of 100 μg/ml. After 5 days of incubation, the

fermentation was collected and the cells were removed by centrifugation at 3,500 g for 10 min.

The supernatant (1000 ml) was first acidized with 75 ml HCl (1.0 M), and then extracted three times with *n*-hexane/dichloromethane/isopropanol (2/1/0.1, v/v/v). The upper organic layer was combined and subjected to a rotary evaporator under vacuum. The residue was reconstituted in methanol. The metabolites were isolated using a Gilson 281 Liquid Handler (Gilson, Paris, France) equipped with a Gilson 322 pump and a Gilson 156 UV detector. Synergi MAX-RP Prep ODS column (150 mm × 30 mm i.d., 4 μm, Phenomenex, Torrance, CA) was employed. Acetonitrile (A) and 10 mM ammonium acetate (B) were used as the mobile phase. The flow rate was set to 25 ml/min and detection was conducted at 230 nm. The gradient elution program was as follows: 0 min, 10% A; 1.5 min, 10% A; 21.8 min, 40% A; 22 min, 100% A; 25 min, 100% A; 25.2 min, 10% A. Several major chromatographic peaks (retention times at 6.2, 6.8, 9.1, 12.8, 19.1, and 22.0 min) were collected using an automatic fraction collector. All fractions of the same peak were combined and evaporated to dryness via lyophilization. The structures of these compounds were confirmed by UPLC-Q/TOF MS, proton nuclear magnetic resonance (^{1}H NMR) and carbon-13 (^{13}C) NMR. The NMR spectra were recorded on a Bruker AVANCE III-400 (Newark, DE) or a Varian INOVA 600 spectrometer (Palo Alto, CA), using tetramethylsilane as an internal standard. Standard compounds were dissolved in deuterated methanol or chloroform. Chemical shifts were expressed as parts per million relative to tetramethylsilane.

DMD Fast Forward. Published on November 20, 2012 as DOI: 10.1124/dmd.112.049684
This article has not been copyedited and formatted. The final version may differ from this version.

Pharmacokinetics of NBP and its Four Major Metabolites in Human Plasma. The concentrations of NBP and its major metabolites, M2, M3-1, M3-2, and M5-2, in human plasma were simultaneously quantified using a sensitive and selective LC-MS/MS method, validated according to FDA guidance, including selectivity, linearity, precision and accuracy, matrix effect, recovery, and stability. Briefly, the analytes and the corresponding synthesized deuterium-labeled internal standards were separated on a Zorbax Eclipse XDB C_{18} column (50 mm × 4.6 mm i.d., 1.8 μm, Agilent, CA) on an Agilent 1200 HPLC system (Agilent, CA). The mobile phase contained methanol-acetonitrile and 5 mM ammonium acetate with the flow rate of 0.6 ml/min. A 6460 triple-quadrupole mass spectrometer (Agilent, CA) operated with an electrospray ionization source was used for mass detection in both negative (for M3-1 and M5-2) and positive (for NBP, M2, and M3-2) modes. The MS parameters were as follows: capillary voltage, +5.0 kV and charging voltage, +0.5 kV; nebulizer gas pressure, 25 psi; carrier gas, 10 l/min and 280 °C; and sheath gas, 6 l/min and 280 °C. Multiple reaction monitoring was employed with following transitions: NBP, *m/z* 191→145; *m/z* M2, 205→145; M3-1, *m/z* 205→161; M3-2, *m/z* 207→128; M5-2, *m/z* 219→175. Calibration curves for NBP and its four major metabolites were fitted via linearly weighted ($1/x^2$) least squares regression. The standard curves ranged from 3.00 ng/ml to 800 ng/ml for NBP and M2, and 3.00 ng/ml to 2400 ng/ml for M3-1, M3-2, and M5-2 in human plasma. The pharmacokinetic parameters were calculated by non-compartmental method using the WinNonlin software (V5.3, Pharsight, Mountain View, CA). The maximum plasma concentration (C_{max}) and the time to

DMD Fast Forward. Published on November 20, 2012 as DOI: 10.1124/dmd.112.049684
This article has not been copyedited and formatted. The final version may differ from this version.

reach C_{max} (T_{max}) were taken directly from the quantification data. The area under the plasma concentration versus time curve (AUC_{0-t}) was calculated from 0 to the last measurable time point (t) based on linear trapezoidal approximation. The terminal elimination rate constant (k_e) was evaluated using the log-linear regression of the plasma concentration during the terminal phase of elimination. Corresponding elimination half-time ($t_{1/2}$) was calculated at $0.693/k_e$. The area under the plasma concentration versus time curve from 0 to infinity ($AUC_{0-\infty}$) was estimated as the sum of (AUC_{0-t}) and C_t/k_e, where C_t is the concentration at the last quantified time point.

Excretion of Metabolites in Human Urine. The concentrations of M3-1 and M5-2 in human urine were determined by UPLC with UV detection at 230 nm. The chromatographic condition for quantification was similar to that for metabolite profiling and identification. Propranolol was selected as internal standard at a concentration of 22.6 μM. Calibration curves for M3-1 and M5-2 were also fitted via linearly weighted ($1/x^2$) least squares regression, and the dynamic curve ranged from 4.85 μM to 388 μM and 4.55 μM to 364 μM for M3-1 and M5-2, respectively, in human urine. Mono-hydroxylated metabolites and their glucuronide conjugates and M8 were semi-quantified using M3-1 as pseudo reference standard. The other urinary products were semi-quantitatively analyzed using the M5-2 calibration curve.

Metabolism of NBP, M3-2, and 11-hydroxy-NBP in HLMs. The HLMs was carefully thawed on ice prior to the experiment. All analytes were dissolved in methanol and diluted with phosphate buffered saline (PBS, pH 7.4) to the desired concentrations. The final methanol concentration did not exceed 0.1%. The analytes

DMD Fast Forward. Published on November 20, 2012 as DOI: 10.1124/dmd.112.049684
This article has not been copyedited and formatted. The final version may differ from this version.

(50 μM) were mixed with HLMs (1.0 mg of protein/ml) in 100 mM PBS and the total incubation volume was 200 μl. After 3 min of preincubation at 37 °C, reduced form of nicotinamide adenine dinucleotide phosphate (NADPH, 2.0 mM) was added to initiate the reactions. After 1 h incubation, the reactions were terminated with an equal volume of ice-cold acetonitrile. NBP was separately incubated in HLMs with general CYP450 inhibitors, SKF525A (10 μM) and ABT (1.0 mM), to identify the enzymatic pathways involved (Sohlenius-Sternbeck et al., 2000; Furnes and Schlenk, 2005). For M3-2, subsequent experiments were conducted in the presence of ABT (1.0 mM). And for 11-hydroxy-NBP, inhibition tests were carried out in the presence of ABT (1.0 mM) and 17-ODYA (10 μM), a potent inhibitor for CYP4A and CYP4F subfamilies (Lasker et al., 2000; Nithipatikom et al., 2004; Jin et al., 2011). Each of the inhibitors was preincubated with HLMs and NADPH for 5 min at 37 ℃ before the reactions were started by the addition of the analytes. The solutions were allowed to react for 1 h and quenched thereafter with ice-cold acetonitrile (200 μl).

Human CYP450 Isoenzymes Phenotyping. The general incubation conditions of NBP with 12 major commercially available human recombinant CYP isoforms (50 pM), CYP1A2, 1B1, 2A6, 2B6, 2C8, 2C9, 2C19, 2D6, 2E1, 3A4, 3A5 or 4A11, were essentially identical to those for HLMs, except that HLMs was replaced by CYP450 individual isoforms. In each P450 isoform incubation system, the UPLC-UV peak areas of the detected metabolites were recorded to determine the contributions of the selected P450 enzymes to the NBP metabolite formation. The peak areas of the metabolites detected in each CYP450 isoform were normalized with the nominal

DMD Fast Forward. Published on November 20, 2012 as DOI: 10.1124/dmd.112.049684
This article has not been copyedited and formatted. The final version may differ from this version.

specific content of the corresponding CYP in native HLMs (Rodrigues, 1999). The sum of the normalized peak areas of one specific metabolite was regarded as "100%". The metabolite formed in each CYP450 isoform was expressed as the percentage of the summed area. The effect of individual CYP450 enzyme specific inhibitors on the formation of hydroxylated metabolites was also evaluated using HLMs. The incubation medium contained NBP (50 μM), HLMs (1.0 mg protein/ml), and chemical inhibitors. CYP450 specific inhibitors, α-naphthoflavone (2.0 μM), diethyldithiocarbamate (50 μM), ticlopidine (24 μM), clomethiazole (24 μM), and ketoconazole (2.0 μM), were employed to determine the involvement of CYP1A2, 2A6, 2B6, 2C19, 2E1, and CYP3A4/5 in the process. Incubations were preincubated for 3 min at 37 °C before the addition of NADPH (2 mM), and then stopped after 1 h by ice-cold acetonitrile (200 μl).

Metabolism of M3-2 and 11-hydroxy-NBP in Human Liver Cytosol. Human liver cytosol catalyzed oxidation was conducted in duplicate at 37 °C in a total volume of 200 μl. The incubation medium contained analytes (50 μM) and human liver cytosol (1.0 mg protein/ml) in 100 mM PBS (pH 7.4). The mixture was preincubated for 3 min. The reactions were then started by adding nicotinamide adenine dinucleotide (NAD, 2.0 mM), and allowed to proceed for 1 h before being stopped by ice-cold acetonitrile (200 μl). Inhibition experiments were performed in the presence of an ADH specific inhibitor, 4-MP with four concentration levels (5 μM, 50 μM, 250 μM, and 1 mM), and ALDH inhibitor disulfiram (50 μM). The inhibitors were preincubated with NAD-supplemented human liver cytosol for 5 min at 37 °C

DMD Fast Forward. Published on November 20, 2012 as DOI: 10.1124/dmd.112.049684
This article has not been copyedited and formatted. The final version may differ from this version.

before the reactions were started by adding the analytes. The reactions were quenched as mentioned previously.

Trapping of 11-aldehyde-NBP in Human Liver Cytosol and HLMs. The 11-hydroxy-NBP (50 μM) was incubated with 1.0 mg/ml of human liver cytosol supplemented with NAD (2.0 mM). Methoxylamine was added at the start of the incubation into a final concentration of 5 mM. The reaction was conducted at 37 ℃ in duplicate and stopped with ice-cold acetonitrile (200 μl) after 1 h of incubation. Similarly, 11-aldehyde-NBP was captured in HLMs in the same manner as in human liver cytosol, except that NAD was replaced by NADPH.

Incubation of NBP and M5-2 in Rat Liver Homogenate. Fresh rat liver homogenate was prepared from male Sprague-Dawley rats as described previously (Bjorge and Baillie, 1991). The incubation mixture in a 50 ml Petri dish contained freshly prepared homogenate (2.5 ml), NADPH (2.0 mM), and NBP (or M5-2, 50 μM) in a total volume of 10 ml. After 1 h of incubation at 37 ℃, the mixture was quenched by ice-cold acetonitrile (10 ml). In the chemical inhibition test, the β-oxidation inhibitor 4-pentenoic acid (4-PA, 1.0 mM), was preincubated with NADPH-fortified fresh homogenate for 5 min before the addition of NBP. For M5-2, subsequent experiments were conducted in the presence of 1.0 mM 4-PA or 1.0 mM L-carnitine, a mitochondrial β-oxidation enhancer (Bjorge and Baillie, 1991).

DMD Fast Forward. Published on November 20, 2012 as DOI: 10.1124/dmd.112.049684
This article has not been copyedited and formatted. The final version may differ from this version.

Results

UPLC-Q/TOF MS Analysis of NBP. The chromatographic and MS fragmentation behaviors of the parent drug were first studied to identify NBP metabolites. The NBP retention time was 18.0 min under the chromatographic conditions employed. In ESI (+) mode, NBP provided a protonated molecule $[M + H]^+$ and sodium adduct ion $[M + Na]^+$ at *m/z* 191.109 and 213.093, respectively. The product ion spectrum of NBP under high collision energy scan was shown in Fig. 1A. Fragment ions at *m/z* 173.098 ($-H_2O$), 145.103 (–HCOOH, 100% abundance), 135.047 ($-C_4H_8$), 131.052 ($-H_2O$ $-C_3H_6$), 117.072 (–HCOOH $-C_2H_4$), 105.074 (C_8H_9), 103.057 (C_8H_7), and 91.057 ($-CO_2$ $-C_4H_8$, C_7H_7) were observed. A tentative fragmentation profile was proposed based on the high resolution mass spectral information (Fig. 1B). Therefore, the NBP fragments were formed predominantly by cleavage on the *n*-butyl side chain and the lactone moiety.

Unfortunately, NBP did not show any response in ESI (–) mode, making the interpretation of some metabolites challenging, which gave more informative fragment ions in ESI (–) than in ESI (+) mode. Thus, plasma, urine and feces samples were detected in both positive and negative modes. Based on the fragmentation patterns, high collision energy mass spectra, and chromatographic behaviors, the detected metabolites were compared with those of the parent compound and available reference standards to elucidate their structures.

NBP Metabolite Profiling and Identification. After being processed using the MDF and dealkylation techniques, 6 and 13 metabolites of NBP were detected in

human plasma in the ESI (+) and ESI (–) modes, respectively (Figs. 2A and 2B); whereas 10 and 17 metabolites of NBP were observed in urine samples in the ESI (+) and ESI (–) modes, respectively (Figs. 3A and 3B). Metabolite profiles in pooled human feces as well as urine samples beyond 24 h post-dose were not shown because only trace amount of metabolites were detected. The MS response alone cannot reflect the relative quantity of the metabolites since metabolic modification of the parent drug changes the polarity and their tendency to form ions in the ESI source, resulting in different ionization efficiency and diverse mass responses. Moreover, several metabolites predominantly displayed sodium adducts ($[M + Na]^+$), making the MS response of protonated molecule ($[M + H]^+$) less reliable for relative quantity comparison among the metabolites. Common metabolic conversions, such as hydroxylation and dealkylation, do not cause sharp changes to the chromophoric groups of the parent compound. Thus, the UV absorbance, rather than MS response, can roughly reflect the relative quantity of the metabolites. Figs. 2C and 3C display the corresponding UPLC-UV chromatograms of the plasma and urine samples. Comparing the plasma UV chromatogram with that of blank plasma (Fig. 2D), predominant circulating metabolites were eluted at 7.8 (M5-2), 11.5 (M2), 11.8 (M3-1), and 12.1 min (M3-2). NBP was not detected because of sensitivity. Likewise, the major urinary metabolites were those with the retention times of 7.8 (M5-2), 8.0 (M10), 8.5 (M9-1), 8.7 (M9-2), and 11.3 min (M9-6) compared with corresponding blank urine (Fig. 3D).

Table 1 lists the detailed information of these metabolites, including the pseudo

DMD Fast Forward. Published on November 20, 2012 as DOI: 10.1124/dmd.112.049684
This article has not been copyedited and formatted. The final version may differ from this version.

molecular ion, proposed elemental composition, retention time, and the characteristic fragment ions. Speculated structures of the metabolites are shown in Fig. 4. The metabolites were named in the order of molecular weight; metabolites with the same molecular weight were named in sequential order of retention time. The identification of the metabolites is as follows.

Parent drug M0. A chromatographic peak at 18.0 min, with an elemental composition of $C_{12}H_{14}O_2$, was detected in human plasma. Its protonated molecular weight was 191.106 Da in ESI (+) mode. The retention time and mass spectral fragmentation patterns were identical to the parent drug, indicating that this component was unmetabolized NBP, designated as M0. M0 was not found in human urine and feces.

Metabolite M1. M1, detected only in urine, was much more hydrophilic than other metabolites, being eluted at an early retention time of 4.2 min. M1 displayed $[M + H]^+$/$[M + Na]^+$ ions at *m/z* 193.050/215.033 in ESI (+) and $[M - H]^-$ ion at 191.035 in ESI (–). The elemental composition of M1 was $C_{10}H_8O_4$, suggesting that two carbon units were removed in M1 compared with the parent drug. In ESI (+), a predominant fragment ion at *m/z* 133.029 was yielded by neutral loss of CH_3COOH from the precursor ion. In ESI (–), consecutive neutral losses of CO_2 molecules were observed, resulting in *m/z* 147.045 ($-CO_2$) and *m/z* 103.056 ($-2CO_2$). M1 was confirmed as phthalide-3-acetic acid by comparing its chromatographic and MS behaviors with the commercially available reference standard.

Metabolite M2. M2 was a major circulating metabolite eluted at 11.5 min. M2

DMD Fast Forward. Published on November 20, 2012 as DOI: 10.1124/dmd.112.049684
This article has not been copyedited and formatted. The final version may differ from this version.

exhibited $[M + H]^+$/$[M + Na]^+$ ions at *m/z* 205.087/227.071 in ESI (+); no MS response was observed in ESI (–). The chemical formula of M2 was $C_{12}H_{12}O_3$, indicative of mono-oxidation with dehydrogenation compared with NBP. The high energy mass spectrum of M2 revealed fragment ions at *m/z* 187.074 ($-H_2O$), 145.063 ($-H_2O$ $-CH_2CO$), and 117.071 ($-CH_3CHO$ $-CO_2$). Among them, *m/z* 117.071 was the same as that of NBP, demonstrating that the *n*-butyl side chain was modified. M2 was further confirmed by comparing its retention time and mass spectrum with the reference standard obtained via microbial transformation as described in *Materials and Methods*. The ^{1}H NMR and ^{13}C NMR data of M2 are listed in Table 2. Comparing the chemical shifts of M2 with NBP, aromatic H and C, C-1, and CH-3 were unchanged; however, those of the *n*-butyl side chain shifted downfield. The phenomenon was especially obvious on CH_3-11, where the H and C signals moved downfield from 0.90 to 2.13 and 13.9 to 30.4, respectively, indicating a carbonyl moiety next to CH_3-11. The appearance of a new carbonyl signal in ^{13}C NMR spectrum (i.e., δ_C 210.6) and the disappearance of two H signals of the *n*-butyl side chain further strengthened the assumption. Therefore, M2 was confirmed as 10-keto-NBP. Fragmentation profile of M2 is proposed in Fig. 1D.

Metabolite M3. M3 exhibited $[M + H]^+$/$[M + Na]^+$ ions at *m/z* 207.104/229.080 in ESI (+). The elemental composition was $C_{12}H_{14}O_3$, indicating mono-oxidation products of NBP. M3 contained four isomers, eluted at 11.8 (M3-1), 12.1 (M3-2), 13.1 (M3-3), and 13.8 min (M3-4). M3-1 and M3-2 were major circulating components and apt to lose one (*m/z* 189.094) and two (*m/z* 171.082) H_2O in ESI (+), illustrating

DMD Fast Forward. Published on November 20, 2012 as DOI: 10.1124/dmd.112.049684
This article has not been copyedited and formatted. The final version may differ from this version.

that the aliphatic hydroxyl group was introduced in either C-3 or the *n*-butyl side chain rather than the benzene ring. The reference standards of M3-1 and M3-2 were isolated and purified from microbial incubations to pinpoint the exact hydroxylation site. The ^{1}H NMR and ^{13}C NMR spectra data of M3-1 and M3-2 are summarized in Table 2. The comparison of chemical shifts between M3-1 and NBP indicated that the aromatic ring and *n*-butyl side chain signals were intact whereas the H-3 signal of NBP (i.e., δ_H 5.47) was missing in M3-1. Meanwhile, C-3 signal moved downfield from 81.4 to 107.5, suggesting that the C-3 of M3-1 was connected to two oxygen atoms. Therefore, M3-1 was confirmed to be 3-hydroxy-NBP, which was also reported as one metabolite of ligustilide, a bioactive ingredient from Rhizoma Chuanxiong, in rat plasma (Yan et al., 2008). The tentative fragmentation pattern of M-3-1 is shown in Fig. 1F. The NMR spectra between NBP and M3-2 were significantly different, as listed in Table 2. The H-10 signal of M3-2 moved downfield from 1.42 to 3.80 and the C-10 signal moved downfield from 22.4 to 67.9, indicating that one hydrogen atom of CH_2-10 was substituted by a hydroxyl group. Stepping downfield of both the C and H signals of CH_3-11 further supported the assumption. Thus, M3-2 was elucidated as 10-hydroxy-NBP. The proposed fragmentation profile of M3-2 is displayed in Fig. 1H. M3-3 and M3-4, two minor metabolites in human plasma, displayed no signal in ESI (–). In ESI (+), almost the same fragment ions were observed for both metabolites, including *m/z* 189.092 ($-H_2O$), 171.081 ($-2H_2O$), 153.070 ($-3H_2O$), 149.061 ($-C_3H_5OH$), 131.050 ($-C_3H_5OH$ $-H_2O$), and 103.055 (C_8H_7). The fragment ions *m/z* 131.050 and 103.055 were the same as those of NBP,

DMD Fast Forward. Published on November 20, 2012 as DOI: 10.1124/dmd.112.049684
This article has not been copyedited and formatted. The final version may differ from this version.

indicating that the hydroxyl group was not attached to the aromatic ring. Based on the fact that the positions of C-3, C-10 and C-11 were occupied by M3-1, M3-2 and 11-hydroxy-NBP respectively, the hydroxyl groups in M3-3 and M3-4 were exclusively attached in positions C-8 or C-9.

Metabolite M4. M4 was detected in human plasma and urine at trace level. M4 was eluted at 11.1 min and exhibited $[M - H]^-$ ion at 207.101 in ESI (–), but none in the ESI (+). Chemical formula of M4 was $C_{12}H_{16}O_3$, suggesting that an H_2O molecule was added to NBP. In ESI (–), a single fragment ion at *m/z* 163.110 was observed, which was generated from the neutral loss of CO_2 (– 43.992 Da). When NBP was incubated in basic aqueous solutions (pH = 10 to 12) at 50 °C for 24 h, most of NBP was converted to M4. When the basic solution containing M4 was acidized below pH 3 with 0.1 M HCl, NBP became the predominant component observed whereas M4 dwindled dramatically. Considering that the lactone moiety was susceptible to pH, M4 was proposed as the lactone-hydrolysis product of NBP.

Metabolite M5. M5-1 and M5-2 were eluted at 5.8 min and 7.8 min, respectively, with $[M - H]^-$ ion at *m/z* 219.067 in ESI (–). In ESI (+), M5-2 showed $[M + H]^+$/$[M + Na]^+$ ions at *m/z* 221.093/243.074, whereas M5-1 gave only $[M + Na]^+$ ion at *m/z* 243.060. The elemental composition of M5-1 and M5-2 was $C_{12}H_{12}O_4$, indicating dioxyganation with dehydrogenation compared with NBP. M5-1 was found in plasma and urine. It yielded several fragment ions at *m/z* 201.052 ($–H_2O$), 175.078 ($–CO_2$), 157.068 ($–CO_2 –H_2O$), 147.046, 131.055, 119.051, and 103.058 in ESI (–). Elemental composition of *m/z* 119.051 and 103.058 were C_8H_7O and C_8H_7, respectively,

DMD Fast Forward. Published on November 20, 2012 as DOI: 10.1124/dmd.112.049684
This article has not been copyedited and formatted. The final version may differ from this version.

suggesting that an oxygen atom was attached to the aromatic ring. M5-1 was also isolated from microbial transformation; however, the amount of M5-1 was insufficient for NMR analysis. Incubation of M2 in HLMs resulted in the trace formation of M5-1, implicating M5-1 being a hydroxylated product of M2. M5-2 was the most abundant metabolite in both human plasma and urine based on the UPLC-UV peak areas (Figs. 2C and 3C). Similar to the fragmentation profile of M1 in ESI (–), M5-2 also exhibited characteristic fragment ions at *m/z* 175.078 ($–CO_2$) and 131.089 ($–2CO_2$), underpinning the existence of two CO_2 moieties in M5-2. The reference standard of M5-2 was isolated and purified from microbial incubation. The ^{1}H NMR and ^{13}C NMR data of M5-2 are listed in Table 2. The H and C signals of CH_2-10 shifted downfield from 1.42 (δ_H) and 22.4 (δ_C) in NBP to 2.37 (δ_H) and 37.4 (δ_C) in M5-2, respectively, suggesting the presence of an electron-withdrawing group in C-11. Notably, the C-11 signal increased dramatically from 13.9 to 179.8, strongly indicating that M5-2 is a carboxylic acid. The disappearance of the H signal in CH_3-11 further enhanced this assumption. Therefore, M5-2 was assigned as NBP-11-oic acid. The oxidation of 11-hydroxy-NBP by Jones reagent yielding M5-2 further supported the structure elucidation. A tentative fragmentation pattern of M5-2 is shown in Fig. 1J.

Metabolite M6. M6-1 and M6-2 were found in human plasma and urine. With the chemical formula of $C_{12}H_{12}O_5$, they displayed $[M + H]^+$/$[M + Na]^+$ ions at *m/z* 237.080/259.057 in ESI (+) and $[M - H]^-$ ion at *m/z* 235.063 in ESI (–). Incubation of M5-2 in NADPH-fortified freshly prepared rat liver homogenate yielded trace amount

DMD Fast Forward. Published on November 20, 2012 as DOI: 10.1124/dmd.112.049684
This article has not been copyedited and formatted. The final version may differ from this version.

of M6-2; no M6-1 was detected, indicating M6-2 might be a hydroxylated product of M5-2. However, we could not exclude the possibility of M6-2 being from dioxygenated metabolites. In ESI (–), M6-2 yielded fragment ions at *m/z* 191.075 and 173.063, which were 15.997 Da larger than those of M5-2, suggesting that the hydroxyl group was attached on the alkyl side chain or C-3 of M5-2. M6-1 exhibited similar MS fragmentation pattern as that of M6-2, and was proposed as a regional isomer of M6-2.

Metabolite M7. Minor metabolites M7-1 (observed in urine) and M7-2 (found in plasma and urine) were eluted at 9.5 min and 12.7 min, respectively. In ESI (–), M7-1 and M7-2 exhibited $[M - H]^-$ ion at *m/z* 285.044 with elemental composition of $C_{12}H_{14}O_6S$. They both formed fragment ion at *m/z* 205.091 by loss of 79.953 Da (SO_3), illustrating M7-1 and M7-2 being sulfates of hydroxylated NBP. Incubation of M3-1 and M3-2 with human liver cytosol supplemented with 3'-phosphoadenosine-5'-phosphosulfate resulted in the trace formation of M7-1 and M7-2, respectively. Tentatively, M7-1 and M7-2 were proposed as the sulfate conjugates of M3-1 and M3-2, respectively.

Metabolite M8. M8, eluted at 14.5 min, was detected only in human urine, and exhibited $[M + H]^+$/$[M + Na]^+$ ions at *m/z* 352.123/374.099 in ESI (+) and $[M - H]^-$ ion at *m/z* 350.099 in ESI (–). The chemical composition of $C_{17}H_{21}NO_5S$ suggested that M8 was an *N*-acetylcysteine ($C_5H_7NO_3S$) conjugate of NBP ($C_{12}H_{14}O_2$). In ESI (–) mode, M8 produced a fragment ion at *m/z* 221.065, corresponding to neutral loss of 129.040 Da ($C_5H_7NO_3$), which further supported the presence of an *N*-acetylcysteine

moiety in M8 (Scholz et al., 2005). The reference substance of M8 was isolated from human urine and subjected to NMR analysis. The NMR data of M8 are listed in Table 2. Comparison of the chemical shifts between NBP and M8 revealed that the *n*-butyl side chain and the aromatic ring signals were unchanged, whereas the H-3 signal of NBP (i.e., δ_H 5.47) disappeared in M8. Moreover, the C-3 signal of M8 stepped downfield to 96.7, which was between those of NBP (δ_C 81.4) and M3-1 (δ_C 107.5), therefore M8 was confirmed as 3-*N*-acetylcysteine-NBP. Structurally, the side chain in both M3-1 and M8 remain unmodified, and incubation of M3-1 in freshly prepared rat liver homogenate supplemented with NADPH and *N*-acetylcysteine yielded minor amount of M8, but similar incubation of NBP did not generate detectable M8. The formation of M8 might be related to the sulfate conjugate of M3-1, which contains a good leaving group. More efforts are currently underway to better understand the formation mechanism of this uncommon metabolite.

Metabolite M9. M9-1 – M9-5 were detected in human plasma and urine, whereas M9-6 was only found in human urine. In ESI (–), M9-1 – M9-6 displayed a major fragment ion at *m/z* 205.086 via neutral loss of 176.032 Da ($C_6H_8O_6$), indicating M9-1 – M9-6 being glucuronide conjugates of NBP monoxides. Characteristic fragment ions at *m/z* 113.024 and 85.029 via cleavage of C-O and C-C bonds of glucuronide moiety further supported the addition of a glucuronide molecule in M9-1 – M9-6. The incubation of M3-1 and M3-2 in HLMs supplemented with uridine 5'-diphosphoglucuronic acid (UDPGA) and alamethicin demonstrated that M3-1 resulted in trace formation of M9-6, and M3-2 led to the generation of M9-1 and

DMD Fast Forward. Published on November 20, 2012 as DOI: 10.1124/dmd.112.049684
This article has not been copyedited and formatted. The final version may differ from this version.

M9-2. Therefore, M9-1/M9-2 and M9-6 were accordingly characterized as the glucuronide conjugates of M3-2 and M3-1, respectively. β-glucuronidase hydrolysis of M9-3 – M9-5 fractions isolated from urine revealed that M9-3/M9-4 and M9-5 were the glucuronide conjugates of M3-3 and M3-4, respectively.

Metabolite M10. M10 was eluted at 8.0 min and detected only in urine. In ESI (+), M10 generated almost the same fragment ions as that of M5-2 with similar abundance. Among these ions, *m/z* 221.082 was 176.039 Da less than the precursor ion, implicating M10 being a glucuronide conjugate. The incubation of M10 fraction isolated from human urine in 0.05 M HCl at 60 °C for 48 h resulted in the formation of M5-2. Therefore, M10 was assigned as the glucuronide conjugate of M5-2.

Metabolite M11. M11-1 and M11-2 exhibited $[M + H]^+$/$[M + Na]^+$ ions at *m/z* 399.121/421.106 and both displayed a major fragment ion at *m/z* 223.092 (31.986 Da larger than $[M + H]^+$ ion of NBP at *m/z* 191.106), which was generated via neutral loss of 176.029 ($–C_6H_8O_6$) from the precursor ion, suggesting M11-1 and M11-2 being glucuronide conjugates of dihydroxylated NBP. M11-1 and M11-2 shared similar fragmentation patterns with fragment ions at *m/z* 205.086 ($–C_6H_8O_6 –H_2O$), 187.076 ($–C_6H_8O_6 –H_2O$), 159.085 ($–C_6H_8O_6 –H_2O$ –HCOOH), 149.066, 131.053, 103.056 (C_8H_7), and 91.054 (C_7H_7). Fragment ions at *m/z* 131.053, 103.056, and 91.054 were the same as those of NBP, M3-3, and M3-4, demonstrating that oxygen atoms were not introduced to the aromatic ring. In addition, *m/z* 149.066 was the same as that observed in M3-3 and M3-4, whereas *m/z* 205.086 and 187.076 were 15.994 Da larger than *m/z* 189.092 and 171.081 from M3-3 and M3-4. Tentatively, M11-1

and M11-2 are formed through hydroxylation of M3-3 and M3-4, followed by glucuronidation.

Pharmacokinetics and Renal Elimination of NBP. After an oral administration of 200 mg NBP soft capsules to four healthy Chinese male volunteers, the concentrations of the parent drug NBP and its four major metabolites (i.e., M2, M3-1, M3-2 and M5-2) in human plasma were simultaneously quantified by a fully validated LC-MS/MS method using corresponding deuterated internal standards. The mean plasma concentration versus time profiles for NBP, M2, M3-1, M3-2 and M5-2 are shown in Fig. 5, and their main pharmacokinetic parameters are presented in Table 3. The peak plasma concentrations (C_{max}) of NBP, M2, M3-1, M3-2 and M5-2 were achieved at approximately 0.75 to 1.50 h post-dose, with mean values of 514, 516, 1370, 1681, and 1568 ng/ml, respectively. The average $AUC_{0-\infty}$ values of NBP, M2, M3-1, M3-2, and M5-2 were 864, 1370, 2478, 8902, and 3529 ng·h/ml, respectively. Therefore, the plasma exposures of M2, M3-1, M3-2 and M5-2 were approximately 1.6-, 2.9-, 10.3-, and 4.1-fold higher than that of NBP. The terminal elimination half-times ($t_{1/2}$) of NBP, M2, M3-1, M3-2 and M5-2 averaged 5.3, 2.3, 9.1, 3.9, and 3.3 h, respectively.

Renal Elimination of NBP. The concentrations of M3-1 and M5-2 in human urine were determined using the UPLC-UV method. Other urinary metabolites were semi-quantified using M3-1 or M5-2 as the pseudo-reference standard. Various metabolites, especially glucuronide conjugates, were recovered in human urine, and the total urinary excretion accounted for 81.6% of the administered dosage. The major

metabolic elimination pathways of NBP were ω-carboxylation (and its glucuronide conjugation) and glucuronide conjugation of NBP monoxides, accounting for 23.4% and 21.3% of the dose, respectively.

Oxidation of NBP in HLMs. Incubation of NBP was performed in HLMs as an initial procedure towards identifying drug metabolizing enzymes. Seven oxidized metabolites were detected in NADPH-supplemented HLMs, as illustrated in Figs. 6B and 6C. The major products were confirmed to be M3-1 and M3-2. M5-2 and M2 were found as minor metabolites, and M3-3 and M3-4 were also observed at trace amounts. MS analysis revealed another moderate metabolite, co-eluted with M3-2 under the employed chromatographic condition. It was confirmed as 11-hydroxy-NBP by comparing to a synthesized reference standard using a different gradient elution program (Supplemental Fig. S1). The yield of 11-hydroxy-NBP was about 20% that of M3-2 in terms of chromatographic area. The C and H signals of the aromatic proportion and CH_2-8 to CH_2-10 in 11-hydroxy-NBP were almost the same as those of NBP, whereas C and H signals of CH_2-11 significantly shifted downfield, as listed in Table 2. Furthermore, four CH_2 moieties were observed in the distortionless enhancement by polarization transfer (DEPT) spectrum.

General CYP450 inhibitors SKF525A or ABT were preincubated with HLMs to evaluate the role of CYP450s in the oxidative metabolite formation of NBP. Compared with the control samples without inhibitors, coincubation of SKF525A strongly inhibited NBP metabolism with obviously decreased formation of M2, M3-1, M3-2, M5-2, and 11-hydroxy-NBP (Fig. 7). The preincubation of ABT with HLMs

DMD Fast Forward. Published on November 20, 2012 as DOI: 10.1124/dmd.112.049684
This article has not been copyedited and formatted. The final version may differ from this version.

also inhibited NBP metabolism to a much larger extent than SKF525A (Fig. 7). This evidence suggests the involvement of CYP450s in the oxidative metabolism of NBP.

CYP450 Isoforms Responsible for NBP Hydroxylation. Further incubation of NBP with NADPH-supplemented individual recombinant human CYP450 enzymes was conducted to investigate which CYP450 enzyme(s) catalyzed NBP hydroxylation. NBP was catalyzed by an array of human CYP450 enzymes to form M3-1 to M3-4 and 11-hydroxy-NBP, as summarized in Table 4. Neither M2 nor M5-2 was detected in the tested isoenzyme incubation. After normalization with regard to the native hepatic abundance, CYP3A4 was the most active enzyme for M3-1 formation, followed by CYP2E1 and CYP3A5. CYP2E1 was the primary enzyme responsible for M3-2 generation, followed by CYP2B6 and 2C19. For M3-3 generation, CYP2E1 was the most efficient enzyme, followed by CYP1A2 and 2A6. Isoforms CYP 2A6 and 2E1 contributed to M3-4 production. CYP 1A2, 2B6, and 2E1 were the principal enzymes involved in the formation of 11-hydroxy-NBP. Specific chemical inhibition tests were performed to better evaluate the relative contribution of each isoform to NBP hydroxylation. The results illustrate that neither of the CYP450 specific inhibitors displayed strong inhibition on the generation of M3-1 to M3-4 and 11-hydroxy-NBP (data not shown), probably because NBP metabolism can be compensated by other isoenzymes via the same or alternative hydroxylation pathways when one particular CYP isoform is inhibited.

Insight into the Formation of M5-2. M5-2 is the principal metabolite in both human plasma and urine. However, M5-2 was only detected as a minor metabolite in

DMD Fast Forward. Published on November 20, 2012 as DOI: 10.1124/dmd.112.049684
This article has not been copyedited and formatted. The final version may differ from this version.

NBP incubation with HLMs which was not commensurate with the scenario in vivo. Carboxylic acid metabolites were generally formed via further oxidation of ω-hydroxylated intermediates by ADH and ALDH. Synthesized 11-hydroxy-NBP was incubated in ADH- and ALDH-rich human liver cytosol to evaluate whether ADH and ALDH participated in M5-2 generation. Our results indicate that approximately 95% of 11-hydroxy-NBP was converted to M5-2 in the presence of NAD. In the absence of NAD, metabolism of 11-hydroxy-NBP was negligible. Selective inhibitors of both enzymes were estimated to further confirm the functions of ADH and ALDH in catalyzing 11-hydroxy-NBP. Fig. 8 shows that the presence of 4-MP (5 μM), a potent ADH inhibitor, moderately inhibited M5-2 formation by 36% and 4-MP at 50 μM showed vigorous inhibition on the M5-2 yield. The presence of 4-MP at 250 μM or above almost completely inhibited M5-2 formation. The presence of disulfiram, an ALDH-specific inhibitor, in human liver cytosol reduced M5-2 formation by 40% (Fig. 8). These results clearly support the involvement of ADH and ALDH in the generation of M5-2 from11-hydroxy-NBP.

Despite the robust activity of ADH and ALDH in mediating M5-2 formation, about 30% conversion of 11-hydroxy-NBP to M5-2 was observed in NADPH-supplemented HLMs using 11-hydroxy-NBP as the substrate. Thus, CYP450s or flavin-containing monooxygenases (FMOs) can also catalyze M5-2 formation. Preheating HLMs at 50 °C for 1 min to inactivate FMOs displayed negligible effects on M5-2 formation, excluding the participation of FMOs. Further inhibition experiment was executed to evaluate the role of CYP450s in M5-2 formation. The presence of ABT in HLMs

inhibited M5-2 formation by approximately 89%. Thus, CYP450s also contributed to the generation of M5-2. However, subsequent incubation of 11-hydroxy-NBP with NADPH-fortified recombinant CYP450 isoforms (CYP1A2, 1B1, 2A6, 2B6, 2C8, 2C9, 2C19, 2D6, 2E1, 3A4, 3A5 and 4A11) only yielded trace amounts of M5-2. The presence of 17-ODYA in HLMs decreased M5-2 formation by 59%, suggesting that the CYP4A or CYP4F subfamilies might be partially responsible for the biotransformation of 11-hydroxy-NBP to M5-2 in HLMs.

Although ALDH was proven to participate in the formation of M5-2 from 11-hydroxy-NBP in human liver cytosol, 11-aldehyde-NBP was not detected directly in the incubation mixture because of its obvious instability. Methoxylamine was utilized as the trapping agent to certify the presence of 11-aldehyde-NBP. The potential oxime derivative was detected in both NAD-supplemented human liver cytosol and NADPH-fortified HLMs (Supplemental Fig. S2), demonstrating that 11-hydroxy-NBP was first oxidized to 11-aldehyde-NBP, followed by subsequent oxidation to M5-2.

Investigation on Metabolic Pathway to M2. Similar to the formation mechanism of M5-2, the ketone metabolite M2 can also be generated in either NAD-supplemented human liver cytosol or NADPH-fortified HLMs using M3-2 as the substrate. The metabolism of M3-2 in human liver cytosol demonstrated that about 4% of M3-2 was converted to M2. The presence of higher 4-MP concentration in human liver cytosol also showed enhanced inhibition on M2 generation (Supplemental Fig. S3), indicating that ADH is a potential contributor to M2

formation.

In a separate test, about 11% of M3-2 transformation to M2 was observed when M3-2 was incubated in HLMs. The addition of ABT in HLMs suppressed M2 formation by up to 61 % (Supplemental Fig. S3), suggesting the involvement of CYP450s in M2 yield.

Elucidation on the Generation of M1. Structurally, M1 is two carbon units shorter than other oxidative metabolites, reminding the possible participation of β-oxidation. NBP Metabolism was investigated in freshly prepared rat liver homogenate to test this assumption. Aside from metabolites M2 and M3-1 to M3-4, two carboxylic acids, namely M5-2 and M1, were observed at lower levels. In the chemical inhibition experiments, preincubation with 4-PA, a β-oxidation inhibitor, potently suppressed M1 formation, which was approximately 75% lower than in control samples without 4-PA (Supplemental Fig. S4). M5-2 production increased by nearly 35% in samples supplemented with 4-PA than that in the control samples. These results indicate the possibility of β-oxidation in M1 formation.

Direct incubation of M5-2 in rat liver homogenate showed that a small fraction of M5-2 was converted to M1. In a separate test, the presence of 4-PA in rat liver homogenate incubated with M5-2 exhibited a 54% decrease in the M1 yield (Supplemental Fig. S4). Freshly prepared rat liver homogenate incubated with M5-2 in the presence of a mitochondrial β-oxidation enhancer, L-carnitine, did not increase M1 formation. Possibly the β-oxidation does not occur within the mitochondria.

DMD Fast Forward. Published on November 20, 2012 as DOI: 10.1124/dmd.112.049684
This article has not been copyedited and formatted. The final version may differ from this version.

Discussion

In the present study, the pharmacokinetics, metabolism, and excretion of NBP were investigated in healthy Chinese male volunteers after a single oral administration of 200 mg NBP. NBP was almost completely absorbed; unchanged NBP was not detected in both human urine and feces. Renal excretion was the major route of elimination with roughly 81.6% of the original dose recovered from urine samples. NBP underwent extensive metabolism in humans after oral administration and generated a total of 23 metabolites in human plasma and urine. Metabolites M2, M3-1, M3-2, and M5-2 constituted the principal circulating metabolites, wherein the $AUC_{0-\infty}$ values were approximately 1.6-, 2.9-, 10.3-, and 4.1-fold higher than that of NBP.

Initial in vitro studies with HLMs suggested that NBP primarily went through hydroxylation on the *n*-butyl side chain and C-3, resulting in the formation of M3-1, M3-2, and 11-hydroxy-NBP; only a minor amount of M5-2 was produced. However, this scenario was rather different from that in vivo. In humans, M5-2 represented the second largest circulating metabolite in terms of $AUC_{0-\infty}$ values; and M5-2, together with its glucuronide conjugate, was the major elimination pathway. Furthermore, the potential precursor of M5-2, 11-hydroxy-NBP, which appeared as a moderate metabolite in HLMs, was not observed in humans after drug administration, indicative of further metabolism to generate secondary metabolites. To better understand the inconsistency between in vitro and in vivo metabolic profiles, the secondary oxidation rates were compared between M3-2 (forming M2) and 11-hydroxy-NBP. The preliminary kinetic analysis revealed that the formation velocities of M2 in

NADPH-supplemented HLMs and NAD-fortified human liver cytosol were 45.0 and 16.2 pmol/min/mg protein, and those of M5-2 were 91.7 and 390 pmol/min/mg protein, respectively. These formation velocities were observed when M3-2 and 11-hydroxy-NBP were set at 50 μM. Based on these data, the secondary metabolic rate ratio of 11-hydroxy-NBP to M3-2 was roughly 2.0 in HLMs, which surged up to 24.1 in human liver cytosol. Similar formation rate ratios of M5-2 to M2 were also observed in HLMs and human liver cytosol when M3-2 and 11-hydroxy-NBP were set at 5 μM. The significantly faster secondary oxidation rate of 11-hydroxy-NBP delivers plausible explanation for its complete disappearance in humans after drug administration. Thus, although 11-hydroxy-NBP is not detected in human plasma and urine after the oral administration of NBP, there is no reason to believe that the mechanism underlying M5-2 formation in vivo differs from the corresponding mechanism in vitro. It seems highly likely that once 11-hydroxy-NBP is formed, it subsequently undergoes further oxidation to generate M5-2 due to the robust activity of human ADH, ALDH, and CYP450s in the liver. Being different from M3-2 and 11-hydroxy-NBP, M3-1 possessed good metabolic stability in HLMs, which partially contributes to the longer half-time of M3-1 in plasma than those of NBP and other major metabolites.

Several drugs with alkyl side chains, such as CI-976, sameridine, and amiodarone, can be metabolized to corresponding carboxylic acids (Sinz et al., 1997; Sohlenius-Sternbeck et al., 2000; Deng et al., 2011). The formation of these metabolites generally involves initial ω-hydroxylation of the alkyl side chain by

CYP450s (Chmela et al., 2001; Walsh et al., 2002; Zollinger et al., 2011) and subsequent oxidation of the ω-hydroxylated metabolites to carboxylic acids by cytosolic ADH and ALDH (Mori et al., 1989; Aasmoe et al., 1998; Walsh et al., 2002; Miura and Ohkubo, 2007; Dalvie et al., 2008). Microsomal CYP450s were also occasionally reported to catalyze this metabolic pathway (Mori et al., 1989; Ling et al., 1995; Martin et al., 2005; Dalvie et al., 2008). In the present study, initial ω-hydroxylation was mediated mainly by CYP1A2, 2B6 and 2E1. In NAD-supplemented human liver cytosol, ω-hydroxy-NBP (11-hydroxy-NBP) was oxidized to 11-aldehyde-NBP by ADH, which underwent sequential catabolism to M5-2 by ALDH. Microsomal CYP450s also played an important role in converting 11-hydroxy-NBP to M5-2. Reaction of 11-hydroxy-NBP in NADPH-supplemented HLMs displayed around 30% of transformation to M5-2. The addition of ABT in HLMs significantly decreased M5-2 formation, pointing to the contribution of CYP450s to the conversion besides ADH and ALDH. Sequential incubations of 11-hydroxy-NBP in a panel of commercially available human recombinant CYP450 isoforms only yielded trace amounts of M5-2, and the presence of 17-ODYA suppressed M5-2 formation by 59%, illustrating that the CYP4A or CYP4F subfamilies partially catalyzed 11-hydroxy-NBP to M5-2 in HLMs. Trapping tests with methoxylamine proved the presence of the 11-aldehyde-NBP intermediate in the incubation mixture of 11-hydroxy-NBP with either human liver cytosol or HLMs. Addition methoxylamine in human liver cytosol showed negligible effects on the M5-2 yield. However, the addition of methoxylamine in HLMs blocked M5-2

formation by 91%. Possibly because the 11-aldehyde-NBP in human liver cytosol was oxidized quickly to M5-2 by potent ALDH but there was a lack of such oxidase in HLMs, which requires further investigation. Besides, M3-2 was also observed to abide by similar metabolic pathways to 11-hydroxy-NBP, i.e., being oxidized by both ADH and CYP450s to form M2.

In vitro experiments illustrated that the side chain-shortened metabolite M1 was generated through β-oxidation from M5-2; the mitochondria was not involved in the process. It has been reported that the β-oxidation pathway involves the participation of ATP, coenzyme A, and carnitine (Bjorge and Baillie, 1991; Silva et al., 2008). The conversion of M5-2 to M1 can compete for these limited pools of cofactors, and to a certain extent, cause some undesirable effects on the metabolism of endogenous lipid and other xenobiotic carboxylic acids. This phenomenon was observed in patients with valproic acid therapy (Kibayashi et al., 1999).

In summary, the present study revealed that NBP was well absorbed and underwent extensive metabolism to multiple oxidative and conjugated metabolites after its oral administration. Hydroxylation was the initial and major route of metabolism, which occurred predominantly on the *n*-butyl side chain and C-3 instead of the aromatic ring. Renal excretion was the primary elimination pathway. Several in vitro approaches demonstrated that multiple enzymes including CYP450s, ADH, and ALDH were involved in the overall clearance of NBP, indicating a low potential of drug-drug interaction in cases of co-administration. However, concerns should be raised on the safety and pharmacodynamic activities of M2, M3-1, M3-2 and M5-2 due to their

higher plasma exposures than that of NBP.

DMD Fast Forward. Published on November 20, 2012 as DOI: 10.1124/dmd.112.049684
This article has not been copyedited and formatted. The final version may differ from this version.

Acknowledgments

We would like thank Dr. Liang Li, Mr. Tieying Zhang and Ms. Shunbo Zhao for their kind help on the purification of metabolites from microbial biotransformation and structural elucidation. We also would like thank the clinical staff of the First Affiliated Hospital of Lanzhou University and the volunteers in this clinical study.

Authorship contributions

Participated in research design: Diao, Chen, Xie, Deng, Zhang, Zhong and Li.

Conducted experiments: Diao, Deng and Li.

Contributed new reagents or analytic tools: Diao, Li and Chen.

Performed data analysis: Diao, Chen, Deng and Xie.

Contributed to the writing of the manuscript: Diao, Chen, Deng, Xie and Zhong.

References

Aasmoe L, Winberg JO, and Aarbakke J (1998) The role of liver alcohol dehydrogenase isoenzymes in the oxidation of glycolethers in male and female rats. *Toxicol Appl Pharmacol* **150:**86-90.

Asha S and Vidyavathi M (2009) Cunninghamella – A microbial model for drug metabolism studies – A review. *Biotechnol Adv* **27:**16-29.

Bjorge SM and Baillie TA (1991) Studies on the beta-oxidation of valproic acid in rat liver mitochondrial preparations. *Drug Metab Dispos* **19:**823-829.

Brenstrum TJ, Brimble MA, and Stevenson RJ (1994) Directed Ortho Metalations of Tertiary Benzamides Using Lactones as Electrophiles. *Tetrahedron* **50:**4897-4904.

Brimble MA, Horner GM, and Stevenson RJ (1996) Synthesis of aromatic spiroacetals. *Aust J Chem* **49:**189-196.

Chmela Z, Vesely J, Lemr K, Rypka M, Hanus J, Havlicek L, Krystof V, Michnova L, Fuksova K, and Lukes J (2001) In vivo metabolism of 2,6,9-trisubstituted purine-derived cyclin-dependent kinase inhibitor bohemine in mice: Glucosidation as the principal metabolic route. *Drug Metab Dispos* **29:**326-334.

Chong ZZ and Feng YP (1999) dl-3-n-butylphthalide improves regional cerebral blood flow after experimental subarachnoid hemorrhage in rats. *Acta Pharmacol Sin* **20:**509-512.

Dalvie D, Chen W, Zhang C, Vaz AD, Smolarek TA, Cox LM, Lin J, and Obach RS

(2008) Pharmacokinetics, metabolism, and excretion of torcetrapib, a cholesteryl ester transfer protein inhibitor, in humans. *Drug Metab Dispos* **36:**2185-2198.

Deng P, You T, Chen X, Yuan T, Huang H, and Zhong D (2011) Identification of amiodarone metabolites in human bile by ultraperformance liquid chromatography/quadrupole time-of-flight mass spectrometry. *Drug Metab Dispos* **39:**1058-1069.

Furnes B and Schlenk D (2005) Extrahepatic metabolism of carbamate and organophosphate thioether compounds by the flavin-containing monooxygenase and cytochrome P450 systems. *Drug Metab Dispos* **33:**214-218.

Jin Y, Zollinger M, Borell H, Zimmerlin A, and Patten CJ (2011) CYP4F Enzymes Are Responsible for the Elimination of Fingolimod (FTY720), a Novel Treatment of Relapsing Multiple Sclerosis. *Drug Metab Dispos* **39:**191-198.

Kibayashi M, Nagao M, and Chiba S (1999) Influence of valproic acid on the expression of various acyl-CoA dehydrogenases in rats. *Pediatr Int* **41:**52-60.

Lasker JM, Chen WB, Wolf I, Bloswick BP, Wilson PD, and Powell PK (2000) Formation of 20-hydroxyeicosatetraenoic acid, a vasoactive and natriuretic eicosanoid, in human kidney. Role of Cyp4F2 and Cyp4A11. *J Biol Chem* **275:**4118-4126.

Li J, Li Y, Ogle M, Zhou X, Song M, Yu SP, and Wei L (2010) DL-3-n-butylphthalide prevents neuronal cell death after focal cerebral ischemia in mice via the JNK

pathway. *Brain Res* **1359:**216-226.

Li N, Wang XL, Li TT, Ji H, Zhang YH, Qiu ZX, Zhao D, and Chen XJ (2011) Identification of circulatory and excretory metabolites of a novel nitric oxide donor ZJM-289 in rat plasma, bile, urine and faeces by liquid chromatography-tandem mass spectrometry. *Xenobiotica* **41:**805-817.

Ling KHJ, Leeson GA, Burmaster SD, Hook RH, Reith MK, and Cheng LK (1995) Metabolism of Terfenadine Associated with Cyp3a(4) Activity in Human Hepatic Microsomes. *Drug Metab Dispos* **23:**631-636.

Martin JW, Mabury SA, and O'Brien PJ (2005) Metabolic products and pathways of fluorotelomer alcohols in isolated rat hepatocytes. *Chem Biol Interact* **155:**165-180.

Miura M and Ohkubo T (2007) Identification of human cytochrome P450 enzymes involved in the major metabolic pathway of fluvoxamine. *Xenobiotica* **37:**169-179.

Mori M, Kawajiri T, Sayama M, Miyahara T, and Kozuka H (1989) Metabolism of 2,4-dinitrotoluene and 2,6-dinitrotoluene, and their dinitrobenzyl alcohols and dinitrobenzaldehydes by Wistar and Sprague-Dawley rat liver microsomal and cytosol fractions. *Chem Pharm Bull (Tokyo)* **37:**1904-1908.

Nithipatikom K, Gross ER, Endsley MP, Moore JM, Isbell MA, Falck JR, Campbell WB, and Gross GJ (2004) Inhibition of cytochrome P450 omega-hydroxylase - A novel endogenous cardioprotective pathway. *Circul Res* **95:**E65-E71.

Peng SH and Zhou TH (1996) [Investigation on in vivo metabolism of n-butyl

phthalide]. *Yao Xue Xue Bao* **31:**780-784.

Peng Y, Sun J, Hon S, Nylander AN, Xia W, Feng Y, Wang X, and Lemere CA (2010) L-3-n-butylphthalide improves cognitive impairment and reduces amyloid-beta in a transgenic model of Alzheimer's disease. *J Neurosci* **30:**8180-8189.

Peng Y, Xing C, Lemere CA, Chen G, Wang L, Feng Y, and Wang X (2008) l-3-n-Butylphthalide ameliorates beta-amyloid-induced neuronal toxicity in cultured neuronal cells. *Neurosci Lett* **434:**224-229.

Rodrigues AD (1999) Integrated cytochrome P450 reaction phenotyping: attempting to bridge the gap between cDNA-expressed cytochromes P450 and native human liver microsomes. *Biochem Pharmacol* **57:**465-480.

Scholz K, Dekant W, Volkel W, and Pahler A (2005) Rapid detection and identification of N-acetyl-L-cysteine thioethers using constant neutral loss and theoretical multiple reaction monitoring combined with enhanced product-ion scans on a linear ion trap mass spectrometer. *J Am Soc Mass Spectrom* **16:**1976-1984.

Silva MFB, Aires CCP, Luis PBM, Ruiter JPN, IJist L, Duran M, Wanders RJA, and de Almeida IT (2008) Valproic acid metabolism and its effects on mitochondrial fatty acid oxidation: A review. *J Inherit Metab Dis* **31:**205-216.

Sinz MW, Black AE, Bjorge SM, Holmes A, Trivedi BK, and Woolf TF (1997) In vitro and in vivo disposition of 2,2-dimethyl-N-(2,4,6-trimethoxyphenyl)dodecanamide (CI-976).

Identification of a novel five-carbon cleavage metabolite in rats. *Drug Metab Dispos* **25:**123-130.

Sohlenius-Sternbeck AK, Chelpin HV, Orzechowski A, and Halldin MM (2000) Metabolism of sameridine to monocarboxylated products by hepatocytes isolated from the male rat. *Drug Metab Dispos* **28:**695-700.

Walsh JS, Reese MJ, and Thurmond LM (2002) The metabolic activation of abacavir by human liver cytosol and expressed human alcohol dehydrogenase isozymes. *Chem Biol Interact* **142:**135-154.

Wang CH, Feng YP, and Wu YL (1997) [A study on the metabolites of dl-3-n-butyphthalide in rats]. *Yao Xue Xue Bao* **32:**641-646.

Xie C, Zhong DF, Yu KT, and Chen XY (2012) Recent advances in metabolite identification and quantitative bioanalysis by LC-Q-TOF MS. *Bioanalysis* **4:**937-959.

Xu HL and Feng YP (2001) [Effects of 3-n-butylphthalide on thrombosis formation and platelet function in rats]. *Yao Xue Xue Bao* **36:**329-333.

Yan CH and Feng YP (1998) [Protective effects of d-, l-, and dl-3-n-butylphthalide on neuronal damage induced by hypoxia/hypoglycemia in cultured rat cortical neurons]. *Yao Xue Xue Bao* **33:**486-492.

Yan CH, Feng YP, and Zhang JT (1998) Effects of dl-3-n-butylphthalide on regional cerebral blood flow in right middle cerebral artery occlusion rats. *Acta Pharmacol Sin* **19:**117-120.

Yan R, Ko NL, Li SL, Tam YK, and Lin G (2008) Pharmacokinetics and Metabolism

of Ligustilide, a Major Bioactive Component in Rhizoma Chuanxiong, in the Rat. *Drug Metab Dispos* **36:**400-408.

Yang H, Hu GY, Chen J, Wang Y, and Wang ZH (2007) Synthesis, resolution, and antiplatelet activity of 3-substituted 1(3H)-isobenzofuranone. *Bioorg Med Chem Lett* **17:**5210-5213.

Zhang HY, Zhang DL, Ray K, and Zhu MS (2009) Mass defect filter technique and its applications to drug metabolite identification by high-resolution mass spectrometry. *J Mass Spectrom* **44:**999-1016.

Zhu M (2006) Detection and Characterization of Metabolites in Biological Matrices Using Mass Defect Filtering of Liquid Chromatography/High Resolution Mass Spectrometry Data. *Drug Metab Dispos* **34:**1722-1733.

Zollinger M, Gschwind HP, Jin Y, Sayer C, Zecri F, and Hartmann S (2011) Absorption and disposition of the sphingosine 1-phosphate receptor modulator fingolimod (FTY720) in healthy volunteers: a case of xenobiotic biotransformation following endogenous metabolic pathways. *Drug Metab Dispos* **39:**199-207.

Figure Legends

Fig. 1. Mass spectra of the reference substances: NBP (A and B), M2 (C and D), M3-1 (E and F), M3-2 (G and H), and M5-2 (I and J), under high collision energy in positive detection mode and their tentative fragmentation profiles.

Fig. 2. Metabolic profiles in pooled human plasma 1 h after the oral administration of 200 mg NBP soft capsules, as detected by Q-TOF MS in positive (A) and negative (B) modes; and UPLC-UV chromatograms of pooled plasma (C) and human blank plasma (D). AU, arbitrary unit.

Fig. 3. Metabolic profiles in pooled urine 0–24 h after the oral administration of 200 mg NBP soft capsules, as detected by Q-TOF MS in positive (A) and negative (B) modes; and UPLC-UV chromatograms of pooled urine (C) and human blank urine (D). AU, arbitrary unit.

Fig. 4. Proposed metabolic pathway of NBP in humans. Glu, glucuronide.

Fig. 5. Mean plasma concentration versus time profiles of NBP, M2, M3-1, M3-2, and M5-2 after the oral administration of 200 mg NBP soft capsules in four healthy Chinese male volunteers.

Fig. 6. In vitro metabolism of NBP in HLMs. (A) UPLC-UV chromatogram of a control incubation performed without NADPH; (B) UPLC-UV chromatogram of an incubation performed with NADPH; (C) UPLC-Q/TOF MS chromatogram of an incubation performed with NADPH.

Fig. 7. Effect of SKF525A (10 μM) and 1-aminobenzotriazole (ABT, 1 mM) on the formation of major NBP metabolites in HLMs. Data are reported as the mean of two separate determinations.

Fig. 8. Effect of 4-methylpyrazole (4-MP, 5 μM, 50 μM, 250 μM and 1 mM) and disulfiram (50 μM) on M5-2 formation from the incubation of 11-hydroxy-NBP in the human liver cytosol supplemented with NAD. Data are reported as the mean of two separate determinations.

Tables

Table 1. Identification of NBP metabolites in human plasma and urine after a single oral administration of 200 mg NBP soft capsules using UPLC-UV/Q-TOF mass spectrometry.

Name	Description	*m/z*		*m/z*	Formula	Retention	Matrix	Fragment ions	
		$[M+H]^+$	$[M+Na]^+$	$[M-H]^-$		time (min)		ESI(+)	ESI(−)
M0	Parent	191.106	213.093	–	$C_{12}H_{14}O_2$	18.0	plasma	173.098, 145.103, 135.047, 131.052, 117.072, 105.074, 103.057, 91.057	–
M1	Phthalide-3-acetic acid	193.050	215.033	191.035	$C_{10}H_8O_4$	4.2	urine	133.029	147.045, 103.056
M2	10-Keto-NBP	205.087	227.071	–	$C_{12}H_{12}O_3$	11.5	plasma, urine	187.074, 145.063, 117.071	–
M3-1	3-Hydroxylation	207.104	229.080	205.086	$C_{12}H_{14}O_3$	11.8	plasma, urine	189.094, 171.085, 161.099, 147.049, 145.104, 143.089, 133.032, 117.073	161.094
M3-2	10-Hydroxylation	207.103	229.083	205.088	$C_{12}H_{14}O_3$	12.1	plasma, urine	189.091, 171.079, 153.071, 145.102, 143.086, 133.031, 128.064, 117.072	161.092
M3-3	8- or 9-Hydroxylation	207.106	229.086	–	$C_{12}H_{14}O_3$	13.1	plasma	189.092, 171.081, 153.070, 149.061, 131.050, 103.055	–
M3-4	8- or 9-Hydroxylation	207.098	229.083	–	$C_{12}H_{14}O_3$	13.8	plasma	189.092, 171.080, 153.070, 149.059, 131.049, 103.055	–
M4	Hydrolysis	–	–	207.101	$C_{12}H_{16}O_3$	11.1	plasma, urine	–	163.110
M5-1	Hydroxylation of M2	–	243.060	219.067	$C_{12}H_{12}O_4$	5.8	plasma, urine	203.072, 185.063	201.052, 175.078, 157.068, 147.046, 131.055, 119.051, 103.058
M5-2	NBP-11-oic acid	221.093	243.074	219.066	$C_{12}H_{12}O_4$	7.8	plasma, urine	203.081, 185.070, 175.080, 159.052, 157.075, 143.059, 131.058, 103.060	175.078, 157.068, 131.089
M6-1	Hydroxylation of M5-2	237.080	259.057	235.063	$C_{12}H_{12}O_5$	5.9	plasma, urine	219.065, 173.067, 143.116, 133.029	217.046, 191.075, 175.040, 173.065, 147.084, 131.053, 103.056, 91.059
M6-2	Hydroxylation of M5-2	237.080	259.059	235.063	$C_{12}H_{12}O_5$	6.3	plasma, urine	219.065, 173.059, 145.063, 133.029, 117.069	217.053, 191.075, 173.063, 145.068, 129.073, 91.057
M7-1	Sulfation of M3-1	–	–	285.048	$C_{12}H_{14}O_6S$	9.5	urine	–	205.091, 161.064
M7-2	Sulfation of M3-2	–	–	285.044	$C_{12}H_{14}O_6S$	12.7	plasma, urine	–	205.087
M8	*N*-acetylcysteine conjugation	352.123	374.099	350.099	$C_{17}H_{21}NO_5S$	14.5	urine	189.095, 171.086, 147.047, 133.032, 117.074, 91.061	221.065, 177.076, 148.037
M9-1	Glucuronidation of M3-2	383.139	405.118	381.119	$C_{18}H_{22}O_9$	8.5	plasma, urine	207.105, 189.093, 171.082, 153.073, 145.104, 143.087, 133.031, 128.066	363.103, 319.118, 205.087, 187.076, 175.025, 157.013, 113.024, 85.029
M9-2	Glucuronidation of M3-2	383.136	405.121	381.119	$C_{18}H_{22}O_9$	8.7	plasma, urine	207.105, 189.093, 171.083, 153.072, 145.105, 143.089, 133.032	363.103, 319.118, 205.087, 187.076, 175.025, 157.013, 113.024, 85.029
M9-3	Glucuronidation of M3-3	383.130	405.122	381.118	$C_{18}H_{22}O_9$	9.3	plasma, urine	207.105, 189.092, 171.079, 153.067, 149.060, 131.052, 103.056	363.123, 319.127, 205.088, 193.038, 175.029, 157.014, 113.026, 85.031
M9-4	Glucuronidation of M3-3	383.144	405.119	381.114	$C_{18}H_{22}O_9$	9.8	plasma, urine	207.105, 189.091, 171.076, 153.072, 149.061, 131.050, 103.057	363.108, 205.089, 193.035, 175.025, 131.035, 113.025, 85.029
M9-5	Glucuronidation of M3-4	383.139	405.123	381.119	$C_{18}H_{22}O_9$	10.3	plasma, urine	207.105, 189.094, 171.081, 149.061, 131.055	363.119, 205.088, 193.036, 175.030, 157.016, 131.036, 113.026, 85.030
M9-6	Glucuronidation of M3-1	383.144	405.116	381.122	$C_{18}H_{22}O_9$	11.3	urine	207.102, 189.090, 171.082, 161.097, 147.043, 143.086, 133.030, 117.070	205.088, 161.099, 113.025, 85.033
M10	Glucuronidation of M5-2	397.121	419.106	395.093	$C_{18}H_{20}O_{10}$	8.0	urine	221.082, 203.074, 185.064, 175.080, 159.044, 157.068, 143.052, 131.052 103.058, 91.057	219.064, 193.034, 175.074, 145.061, 113.023
M11-1	Dihydroxylation + glucuronidation	399.121	421.106	397.114	$C_{18}H_{22}O_{10}$	6.7	urine	223.092, 205.086, 187.076, 159.085, 149.066, 131.053, 103.056, 91.054	221.078
M11-2	Dihydroxylation + glucuronidation	399.129	421.115	397.111	$C_{18}H_{22}O_{10}$	7.1	urine	223.103, 205.092, 187.083, 159.088, 149.066, 131.055, 103.058, 91.058	221.084

Table 2. ^{1}H NMR and ^{13}C NRM data of NBP, 3-hydroxy-NBP, 10- hydroxy -NBP, NBP-11-oic acid, 10-keto-NBP, 11- hydroxy –NBP, and 3-*N*-acetylcysteine-NBP (*Chemical shifts of the *N*-acetylcysteine moiety are not shown).

Position	NBP		3-hydroxy-NBP		10-hydroxy-NBP		NBP-11-oic acid		10-keto-NBP		11-hydroxy-NBP		3-*N* -acetylcysteine-NBP(*)	
	δC	δH(J/Hz)	δC	δH(J/Hz)	δC	δH(J/Hz)	δC	δH(J/Hz)	δC	δH(J/Hz)	δC	δH(J/Hz)	δC	δH(J/Hz)
1	170.7		168.4		172.8		175.1		172.9		172.9		170.5	
2														
3	81.4	5.47(1H, dd, 7.9, 4.1)	107.5		83.1	5.66(1H, dd, 7.6, 3.9)	85.5	5.61(1H, dd, 6.8, 3.9)	82.8	5.60(1H, dd, 8.0, 3.1)	83.8	5.60(1H, dd, 7.7, 3.9)	96.7	
4	125.6	7.43(1H, dd, 7.7, 0.7)	125.5	7.57(1H, m)	126.2	7.59(1H, m)	128.7	7.59(1H, m)	126.8	7.60(1H, m)	126.7	7.58(1H, m)	126.2	7.56(1H, m)
5	129.0	7.67(1H, td, 7.5, 1.0)	130.5	7.70(1H, t, 6.7)	130.4	7.79(1H, t, 7.5)	133.5	7.76(1H, td, 7.6, 1.0)	131.0	7.76(1H, t, 7.3)	130.8	7.75(1H, td, 7.7, 1.1)	131.3	7.75(1H, m)
6	121.7	7.52(1H, t, 7.5)	122.2	7.57(1H, m)	123.4	7.62(1H, t)	125.9	7.59(1H, m)	124.0	7.62(1H, m)	123.9	7.58(1H, m)	123.9	7.61(1H, m)
7	133.9	7.89(1H, d, 7.7)	134.6	7.86(1H, t, 11.9)	135.6	7.87(1H, d, 7.6)	138.1	7.85(1H, d, 7.6)	136.2	7.85(1H, d, 7.5)	136.1	7.84(1H, d, 7.7)	136.4	7.85(1H, m)
8	34.4	2.06(1H, m)	38.6	2.21(1H, m)	34.8	2.18(1H, m)	37.1	2.17(1H, m)	30.0	2.42(1H, m)	35.9	2.14(1H, m)	31.5	2.15(2H, m)
		1.76(1H, m)		2.08(1H, m)		1.91(1H, m)		1.75(1H, m)		1.90(1H, m)		1.77(1H, m)		
9	26.8		25.3		31.8	1.59(1H, m)	24.0	1.70(2H, m)	39.6	2.71(1H, m)	22.8		27.0	
		1.42(4H, m)		1.29(4H, m)		1.46(1H, m)				2.58(1H, m)		1.52(4H, m)		1.24(4H, m)
10	22.4		22.4		67.9	3.80(1H, m)	37.4	2.37(2H, t, 6.8)	210.6		33.7		23.3	
11	13.9	0.90(3H,t)	13.8	0.86(3H, t, 7.2)	23.5	1.20(3H, d, 6.2)	179.8		30.4	2.13(3H, s)	63.1	3.54(2H, t, 6.2)	14.1	0.78(3H, t, 7.2)
12	151.4		148.8		151.8		154.1		151.8		152.3		151.3	
13	126.1		126.7		127.0		129.4		127.4		127.5		127.5	

DMD Fast Forward. Published on November 20, 2012 as DOI: 10.1124/dmd.112.049684
This article has not been copyedited and formatted. The final version may differ from this version.

Table 3. Pharmacokinetic parameters (mean ± S.D.) of NBP and its four major metabolites in the plasma after a single administration of 200 mg NBP soft capsules to four healthy Chinese volunteers. S.D., standard deviation.

Parameters	NBP	M2	M3-1	M3-2	M5-2
C_{max} (ng/mL)	514 ± 124	516 ± 141	1370 ± 750	1681 ± 187	1568 ± 108
T_{max} (h)	0.75 ± 0.29	1.00 ± 0.00	0.75 ± 0.29	1.50 ± 0.41	1.00 ± 0.00
AUC_{0-t} (ng·h/mL)	831 ± 258	1336 ± 349	2478 ± 1165	8879 ± 2300	3510 ± 867
$AUC_{0-\infty}$ (ng·h/mL)	864 ± 274	1370 ± 354	2525 ± 1164	8902 ± 2292	3529 ± 878
$t_{1/2}$ (h)	5.33 ± 4.27	2.29 ± 0.26	9.09 ± 2.57	3.93 ± 0.31	3.25 ± 2.10

DMD Fast Forward. Published on November 20, 2012 as DOI: 10.1124/dmd.112.049684
This article has not been copyedited and formatted. The final version may differ from this version.

Table 4. Formation of M3-1 to M3-4 and 11-hydroxy-NBP catalyzed by recombinant CYP enzymes.

P450	M3-1 (%)[a]	M3-2 (%)	M3-3 (%)	M3-4 (%)	11-hydroxy-NBP (%)
1A2	n.d.[b]	5.6	32	15	26
2A6	11	3.4	28	43	12
2B6	7.6	28	n.d.[b]	n.d.[b]	25
2C8	2.7	1.1	n.d.[b]	n.d.[b]	2.6
2C9	4.8	2.0	n.d.[b]	n.d.[b]	6.7
2C19	0.9	27	n.d.[b]	n.d.[b]	3.6
2D6	0.5	1.3	2.0	n.d.[b]	9.8
2E1	30	31	37	42	13
3A4	40	n.d.[b]	n.d.[b]	n.d.[b]	n.d.[b]
3A5	20	n.d.[b]	n.d.[b]	n.d.[b]	n.d.[b]
4A11	n.d.[b]	n.d.[b]	n.d.[b]	n.d.[b]	n.d.[b]

[a] The chromatographic peak area of the metabolites detected in individual recombinant CYP450 isoform was normalized with respect to the nominal specific content of the corresponding CYP in native HLMs. Each CYP450 isoform is expressed as the percentage of the total normalized peak area.

[b] n.d: denotes not detected.

Fig. 1.

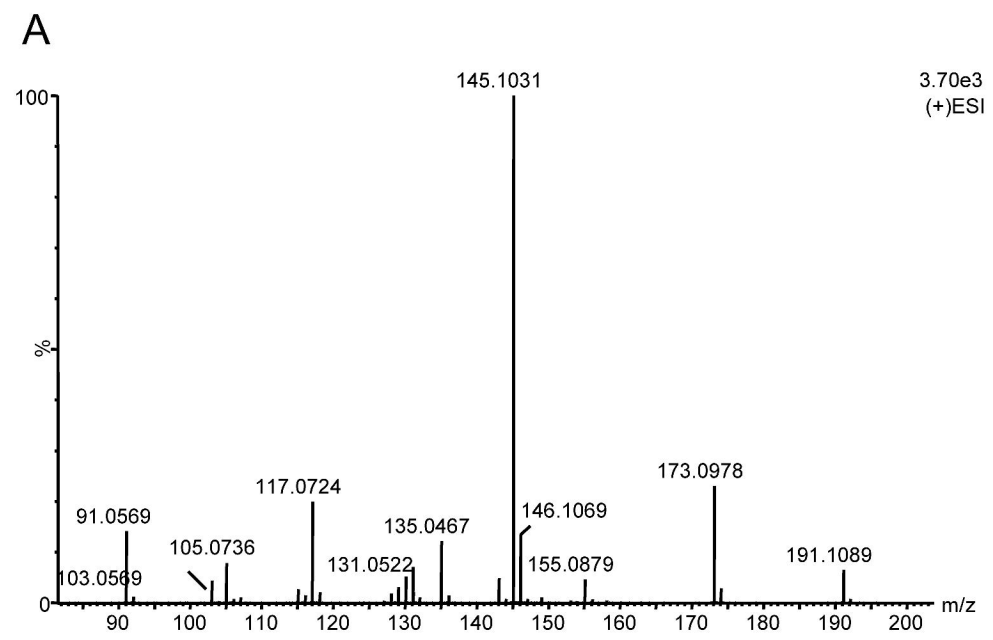

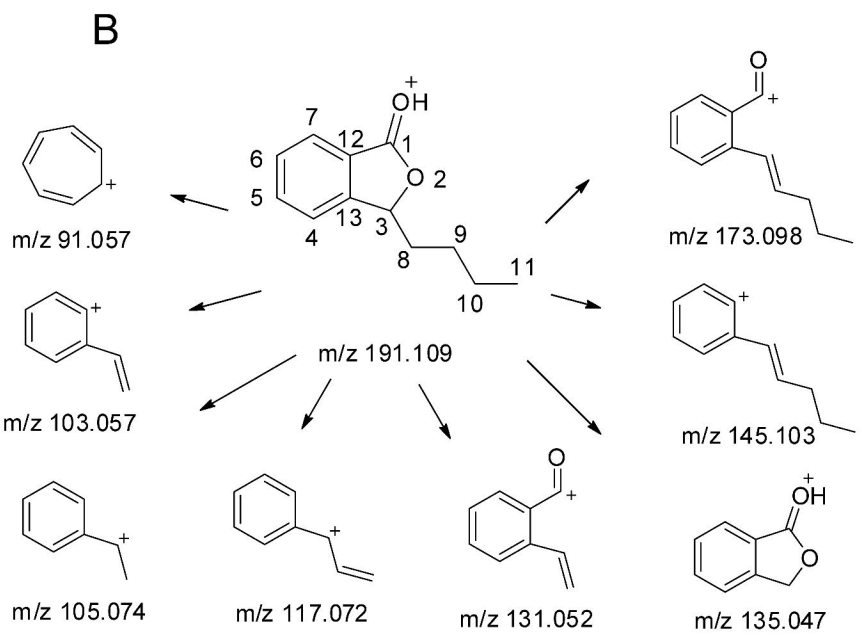

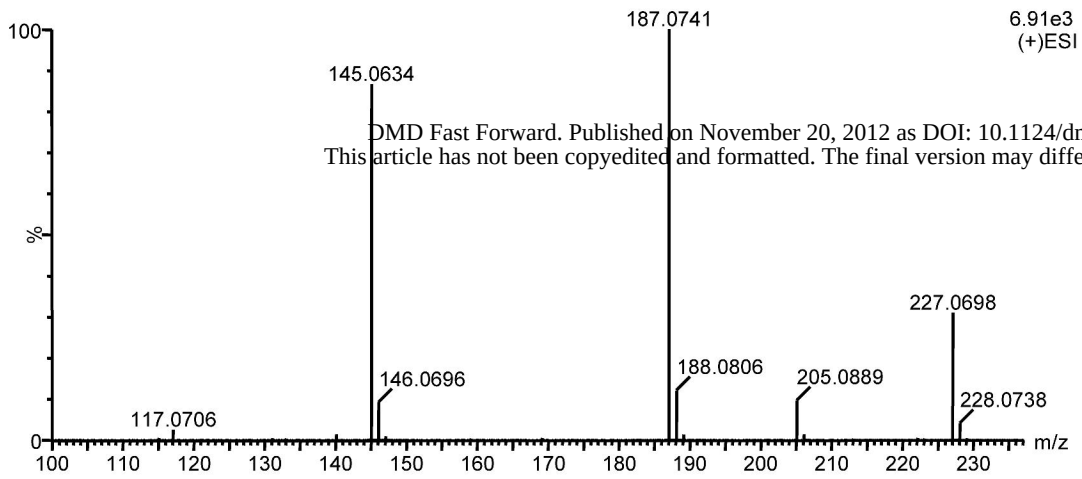

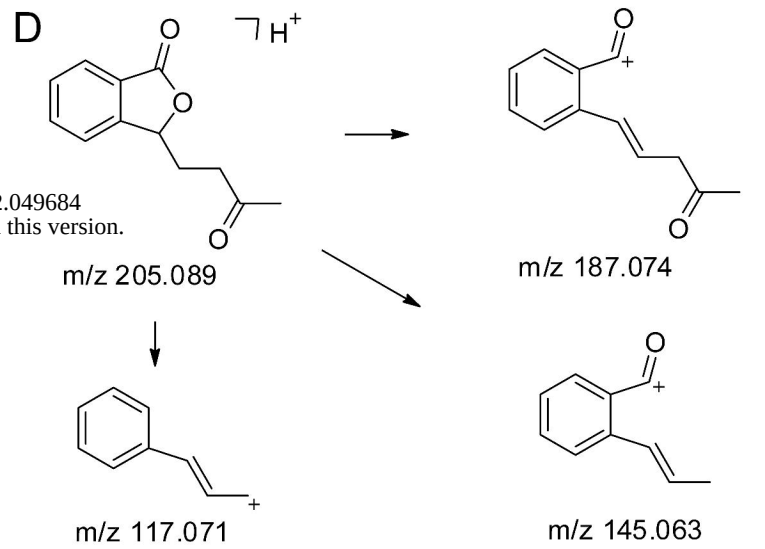

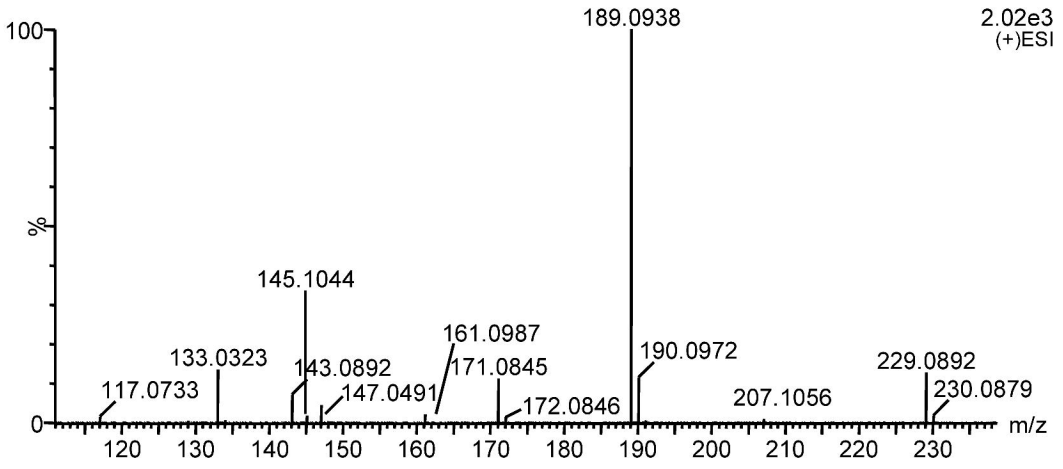

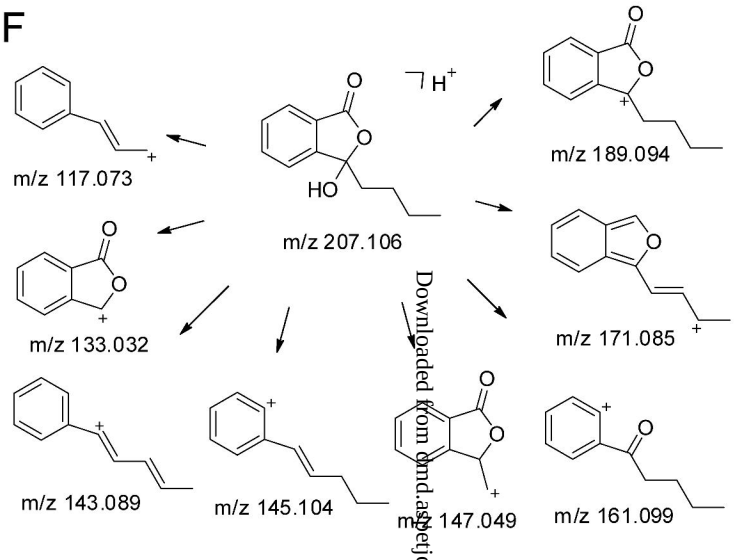

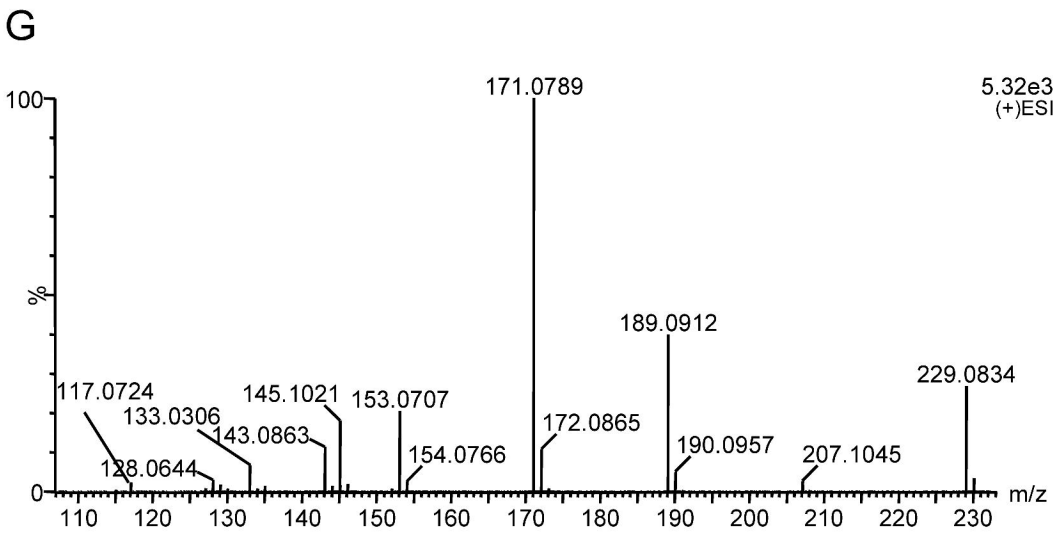

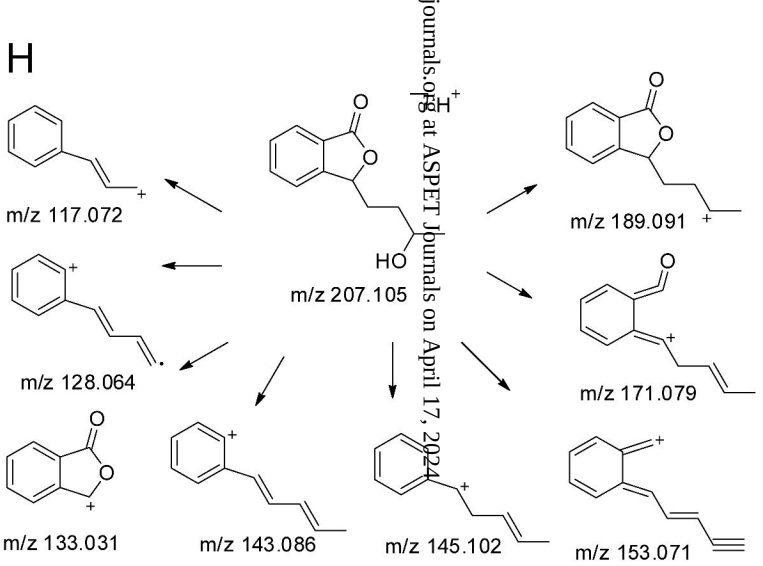

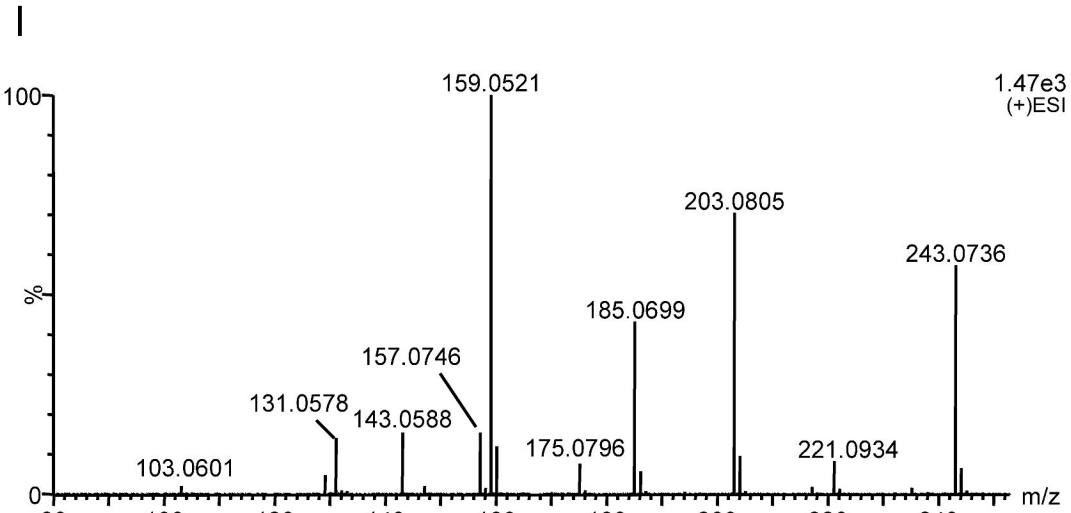

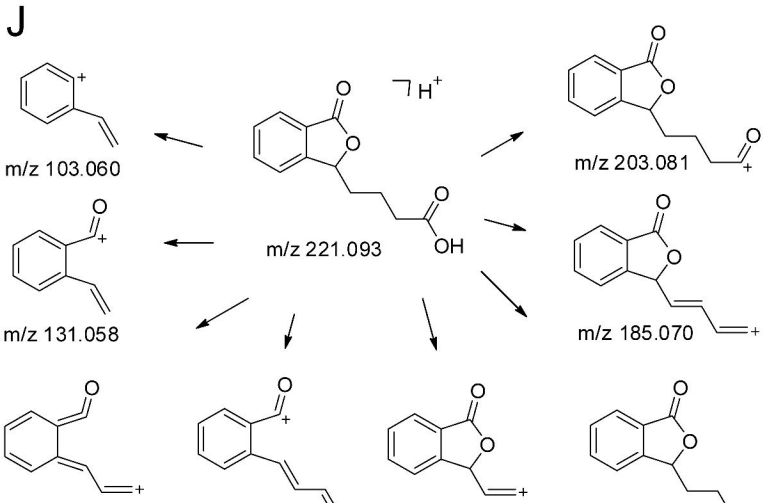

Fig. 2.

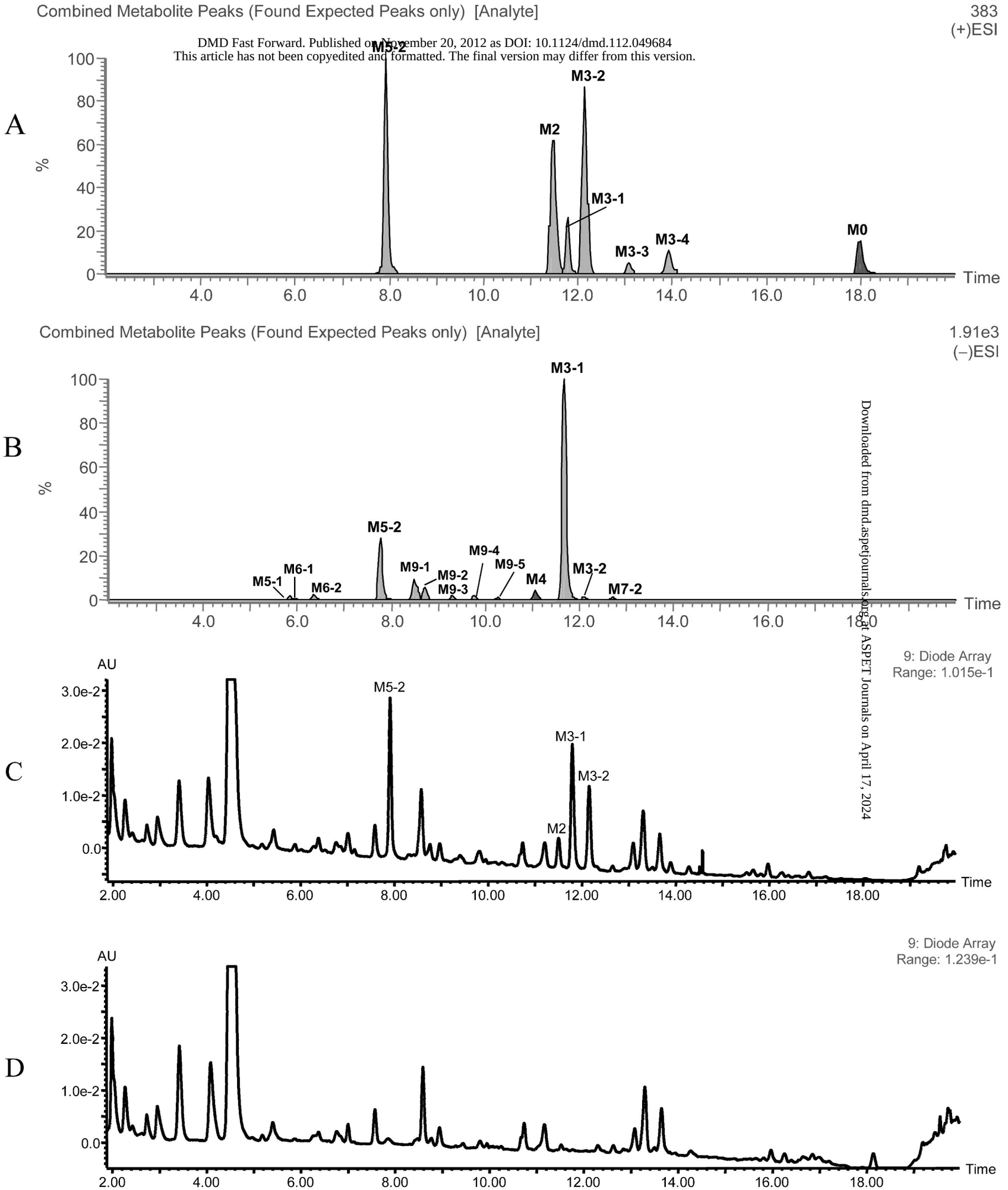

Fig. 3.

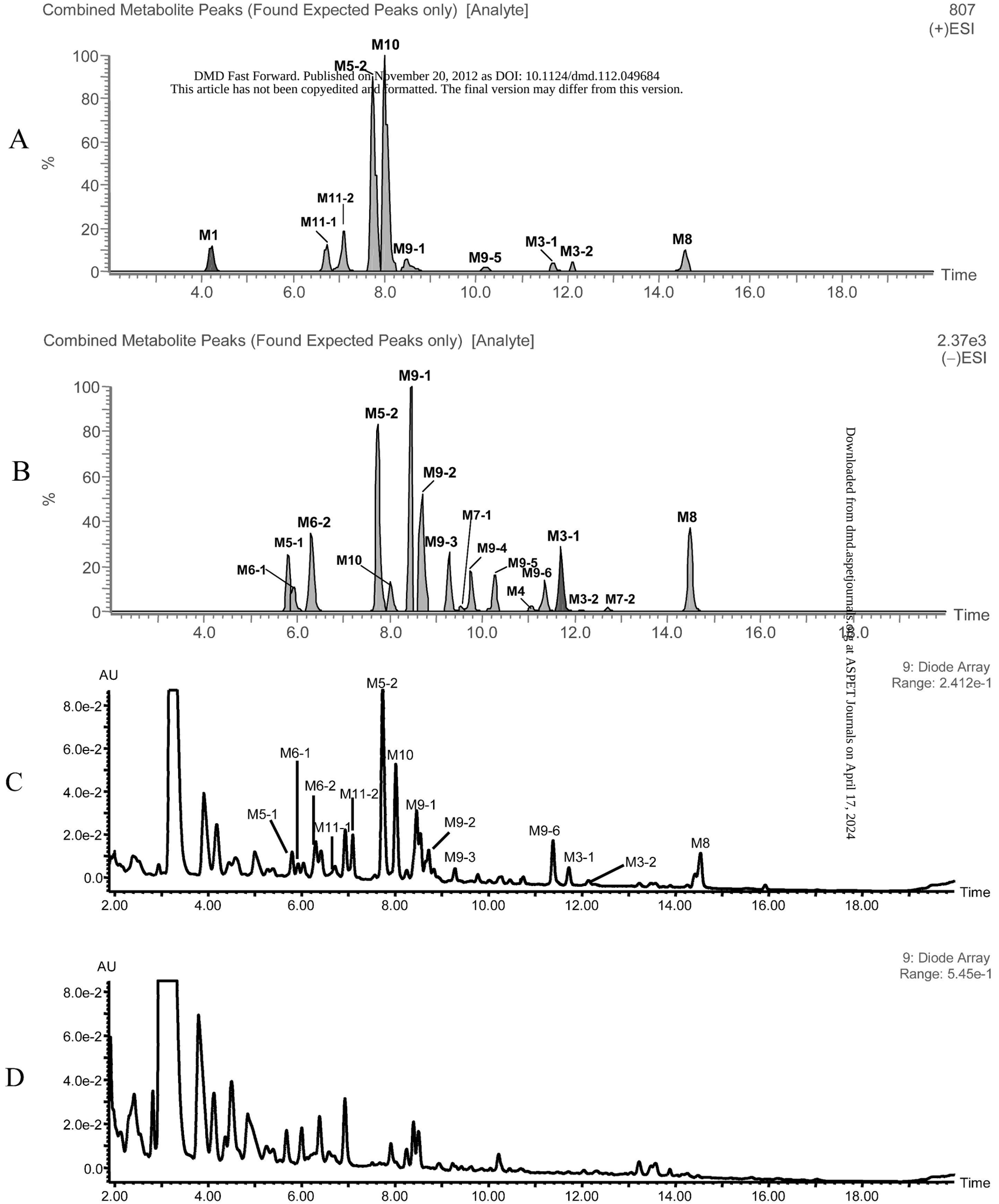

DMD Fast Forward. Published on November 20, 2012 as DOI: 10.1124/dmd.112.049684
This article has not been copyedited and formatted. The final version may differ from this version.

Fig. 4.

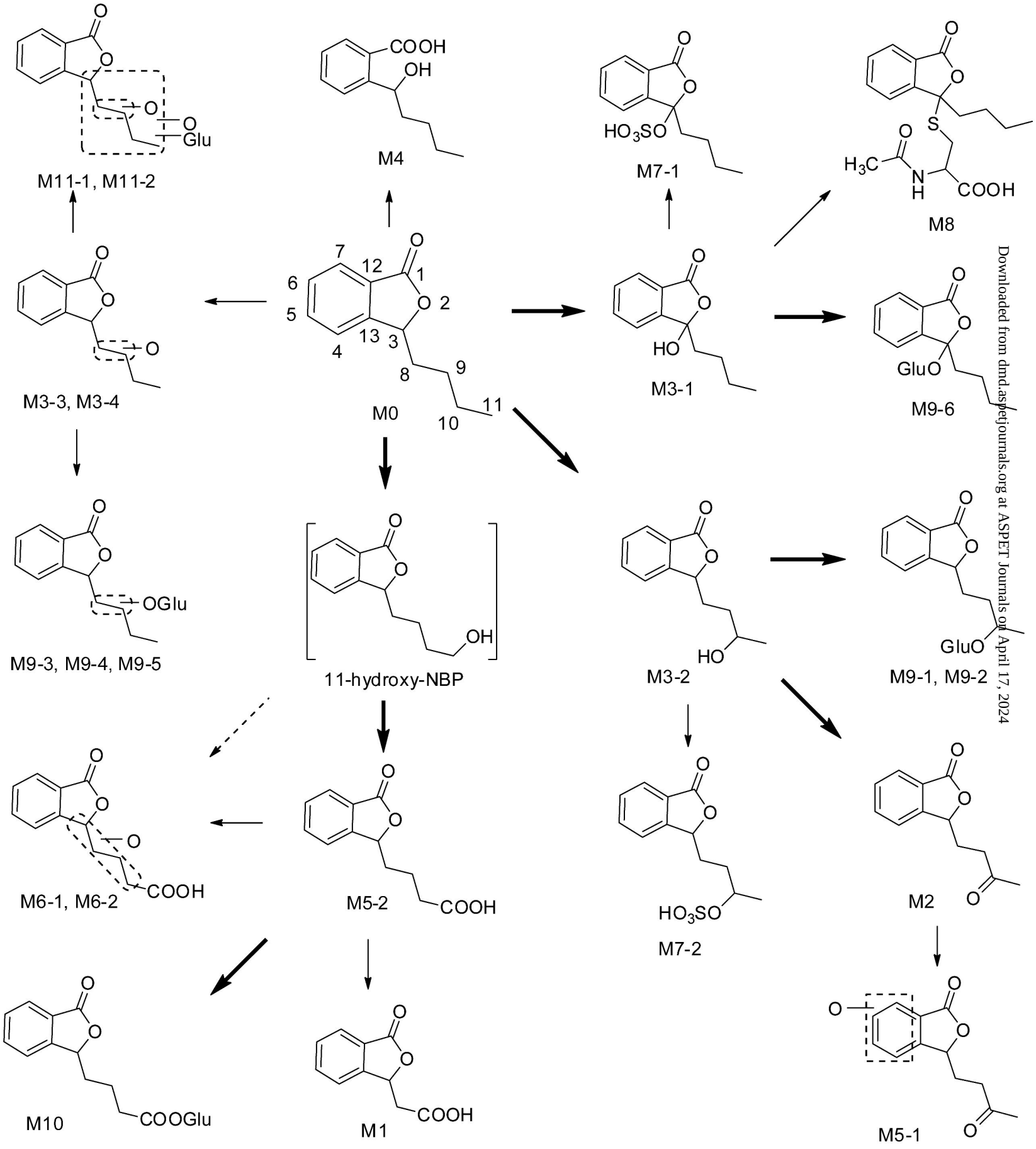

Fig. 5.

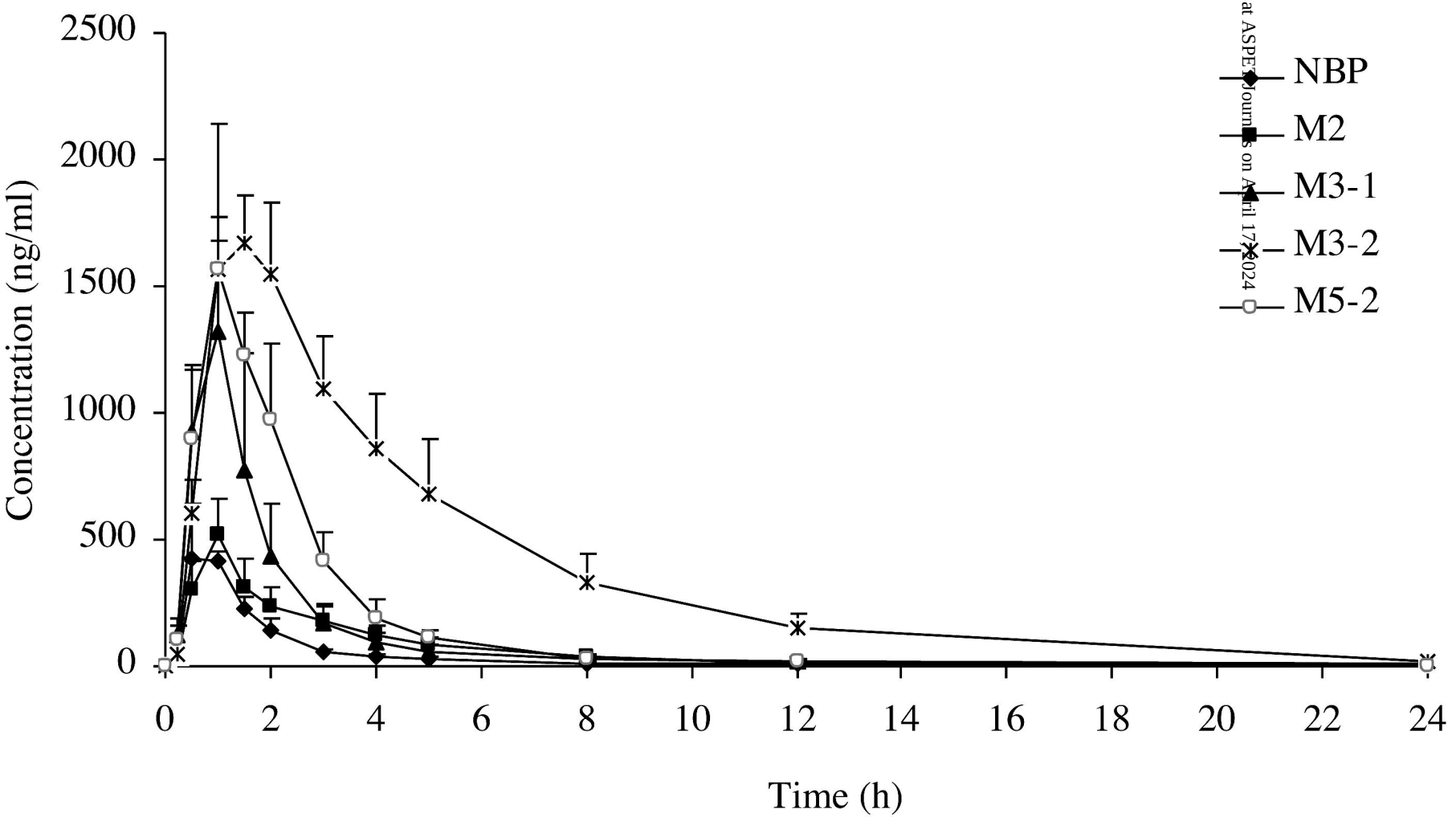

Fig. 6.

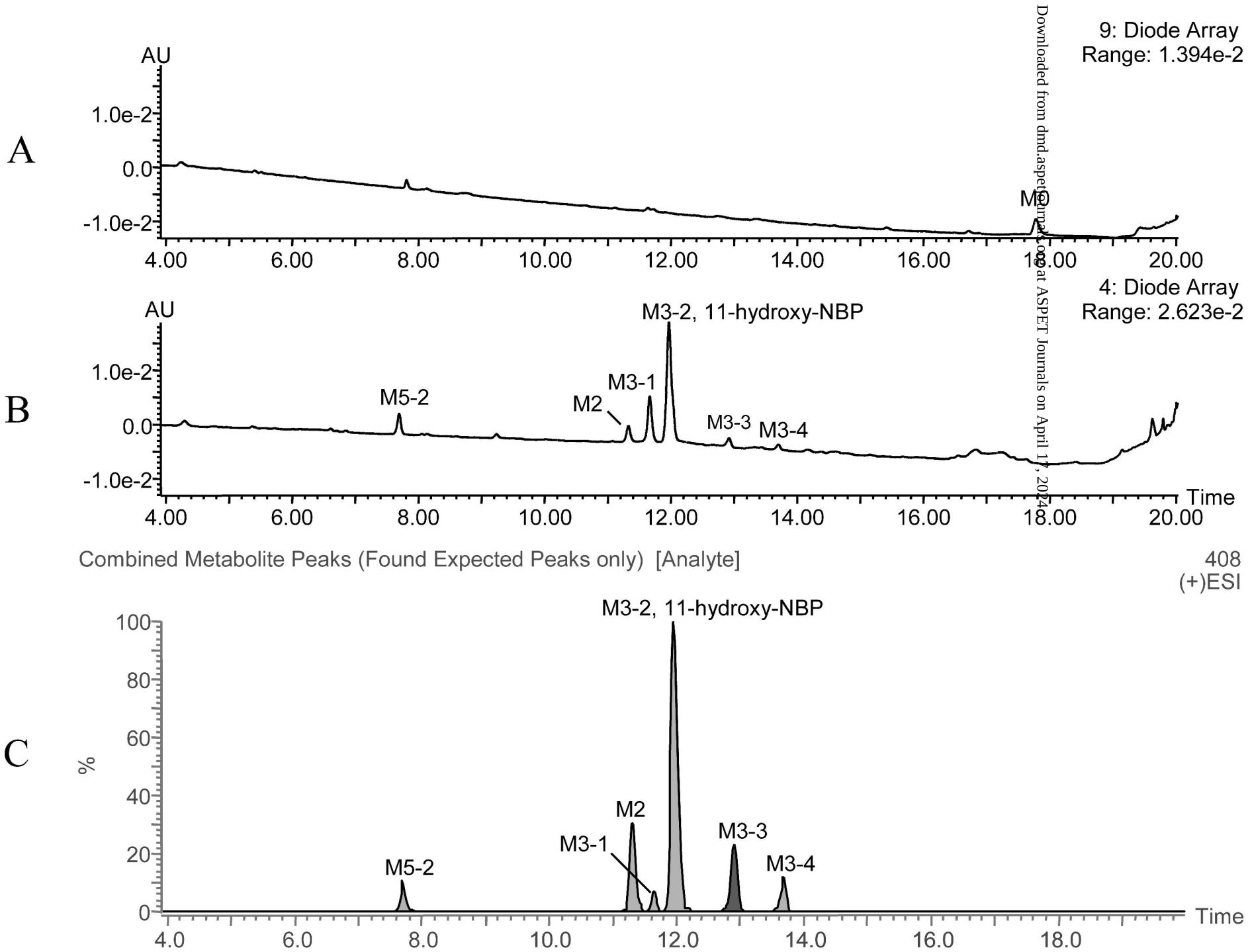

Fig. 7.

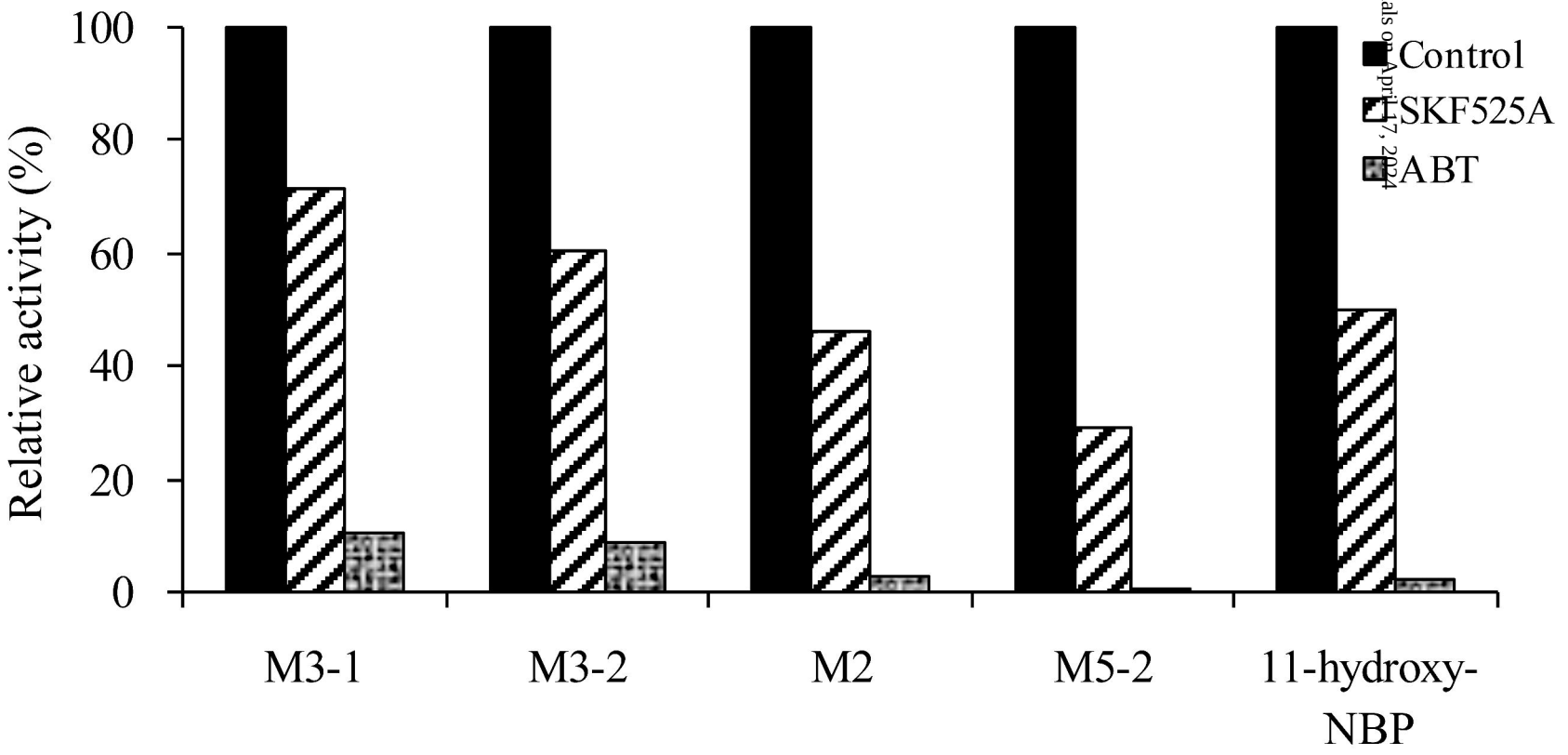

Fig. 8.

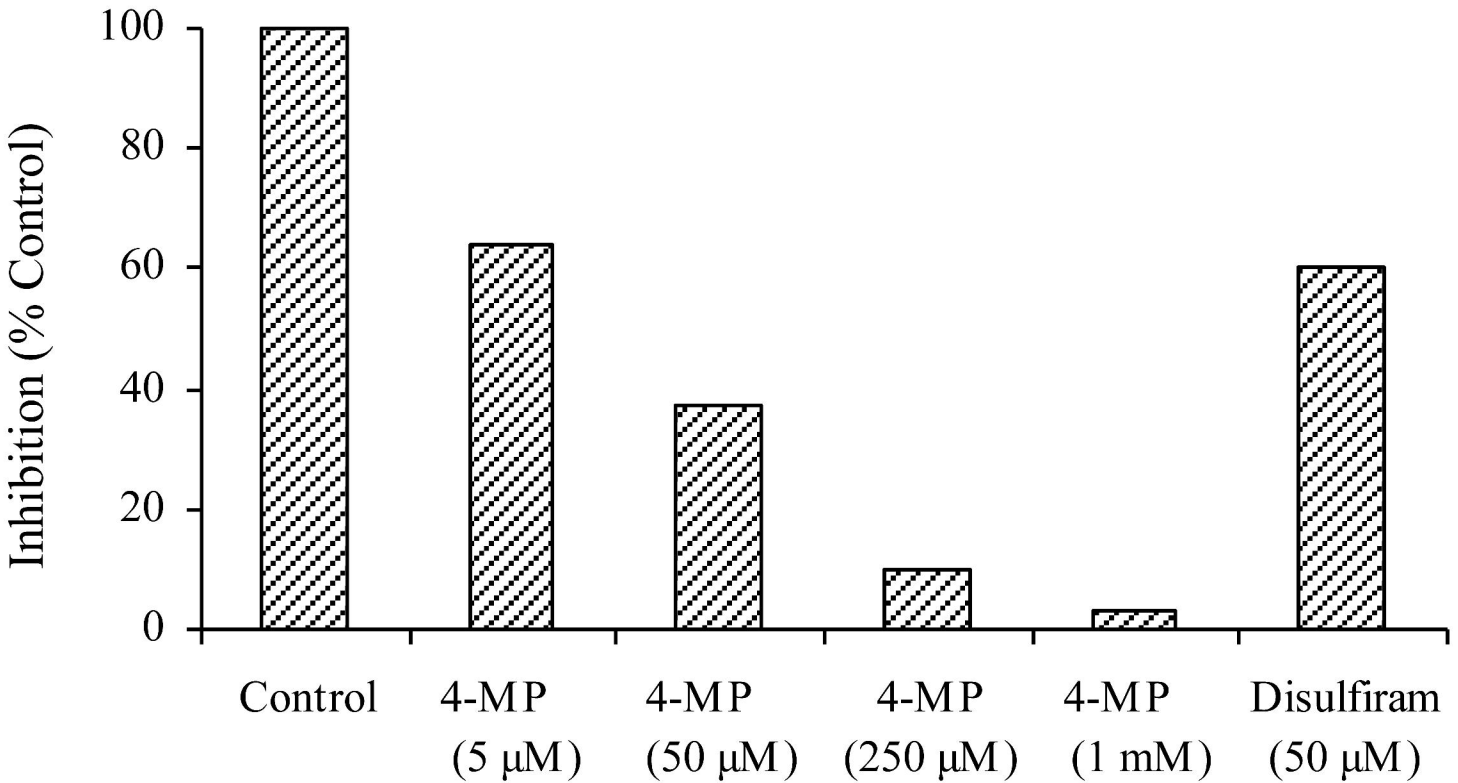
Inhibition (% Control)
100
80
60
40
20
0
Control
4-MP (5 μM)
4-MP (50 μM)
4-MP (250 μM)
4-MP (1 mM)
Disulfiram (50 μM)